


Geochronology and geochemistry of the five magmatic rocks in the Ningzhen region, China

Shunfu Lu^{1,2}  · Xiaoqing Zhu¹ · Xiaofen Li³

Received: 28 December 2017 / Revised: 30 November 2018 / Accepted: 8 January 2019 / Published online: 11 February 2019
© Science Press and Institute of Geochemistry, CAS and Springer-Verlag GmbH Germany, part of Springer Nature 2019

Abstract The Ningzhen region of China is located in the easternmost part of the middle-lower Yangtze River Cu–Fe polymetallic metallogenic belt. From west to east, it comprises five main intermediate–acidic intrusive complexes: the Qilinmen, Anjishan, Xiashu–Gaozi, Shima, and Jianbi complexes. Geochemical investigations show that these five intrusive complexes exhibit high contents of SiO₂, at 64.74–73.40 wt%, Al₂O₃, at 14.15–17.37 wt%, and K₂O + Na₂O, at 6.49–8.68 wt%. The majority of the samples belong to the high-K calc-alkaline series, with a few samples plotting in the calc-alkaline and tholeiitic series. Trace element analysis shows that the samples are enriched in large ion lithophile elements (LILE) and are depleted in high field strength elements (HFSE). The chondrite-normalized rare earth element (REE) patterns are characterized by right-inclined curves, showing light rare earth element (LREE) enrichment. In addition, the (La/Yb)_N ratios are high at 15.02–37.28, with an average of 29.13, and slightly negative or none Eu anomalies are present. In the (La/Yb)_N–δEu diagram, the samples plot within the crust-mantle type field. Laser ablation–inductively coupled plasma–mass spectrometry (LA–ICP–MS) zircon U–Pb dating yielded ages of 122.0 ± 1.0 Ma, 106.1 ± 0.8 Ma, 108.7 ± 1.4 Ma,

103.5 ± 1.9 Ma, and 96.8 ± 1.7 Ma for the Qilinmen, Anjishan, Xiashu–Gaozi, Shima, and Jianbi complexes, respectively. On the basis of this research and knowledge of several known metal deposits related to these complexes, we suggest that the Mesozoic large-scale diagenesis and metallogenesis in the Ningzhen region may have ceased at 100 Ma or about 95 Ma.

Keywords Intermediate–acidic intrusive complexes · LA–ICP–MS zircon U–Pb dating · Geochemistry · Geodynamic setting · Ningzhen region

1 Introduction

The middle–lower Yangtze River belt constitutes one of the most important metallogenic belts in China. This metallogenic belt hosts a large number of polymetallic deposits and includes several main types of ore systems including Cu–Mo porphyry, Cu–Fe skarn, and strata-bound deposits (Pan and Dong 1999; Mao et al. 2006, 2011). The Ningzhen region in Jiangsu Province is located in the easternmost part of the middle-lower Yangtze River belt, where Mesozoic intermediate–acidic intrusive complexes are extensively developed. These intermediate–acidic intrusive complexes, listed in succession from west to east, form the Qilinmen, Anjishan, Xiashu–Gaozi, Shima, and Jianbi intrusive complexes (Fig. 1). Many previous petrological and geochemical studies have been performed on the complexes of the Ningzhen region (Mao and Zhao 1990; Xu et al. 2001). In recent years, studies on the Qilinmen (Chen et al. 2017), Anjishan (Zeng et al. 2013; Liu et al. 2014; Wang et al. 2014a, b; Guan et al. 2015), Gaozi (Sun et al. 2013), Shima (Sun et al. 2013; Guan et al. 2015), and Jianbi (Chen et al. 2017) complexes have

✉ Xiaoqing Zhu
zhuxiaoqing@mail.gyig.ac.cn

¹ State Key Laboratory of Ore Deposit Geochemistry, Institute of Geochemistry, Chinese Academy of Sciences, Guiyang 550081, Guizhou, China

² University of Chinese Academy of Sciences, Beijing 100049, China

³ Earthquake Administration of Hubei Province, Wuhan 430071, Hubei, China

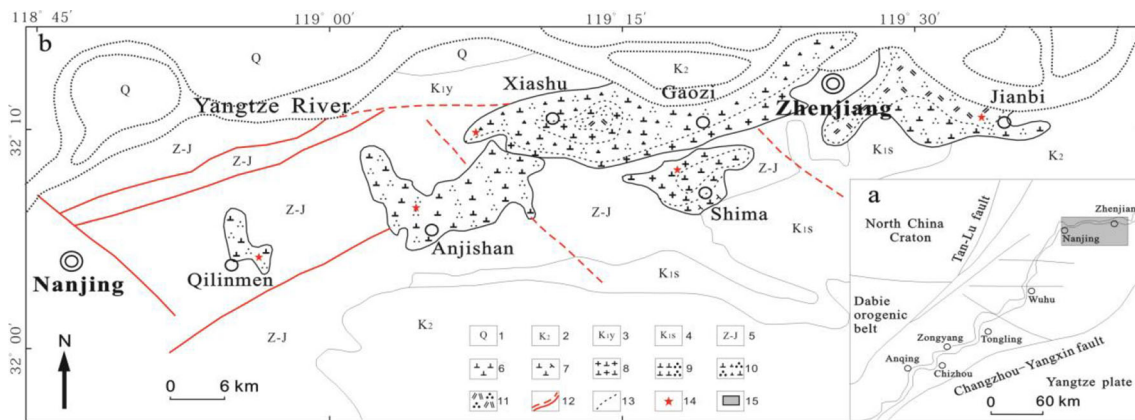


Fig. 1 **a** Tectonic map and **b** distribution of Mesozoic complexes in the Ningzhen region (Xia 2000; Zeng et al. 2013). 1. Quaternary. 2. Upper Cretaceous. 3. Cretaceous Yangchong Formation. 4. Cretaceous Shangdang Formation. 5. Sinian to Jurassic. 6. Diorite. 7. Diorite porphyrite. 8. Granodiorite. 9. Quartz diorite. 10. Quartz diorite porphyrite. 11. Quartz monzonite. 12. Conjectural and actual fractures. 13. Lithofacies boundary. 14. Sampling location. 15. Ningzhen region

obtained highly precise and accurate ages. In this study, we use laser ablation–inductively coupled plasma–mass spectrometry (LA–ICP–MS) zircon U–Pb dating of the five main intermediate–acidic intrusive complexes combined with known highly precise and accurate ages of the other metal deposits in this region to constrain the age of the large-scale mineralization in this region. The geochronology is the key to understanding the geodynamic setting and tectonic evolution as well as the Mesozoic metallogenic processes and is used to confirm the relationship of the ore deposits and intrusive magmatic activity in this region. By analyzing the major and trace element contents in the complexes, this paper presents preliminary discussions on the regional magma sources and evolution processes that occurred in the Ningzhen region and offers an in-depth discussion on the regional geodynamic setting and its geological significance.

2 Geological setting

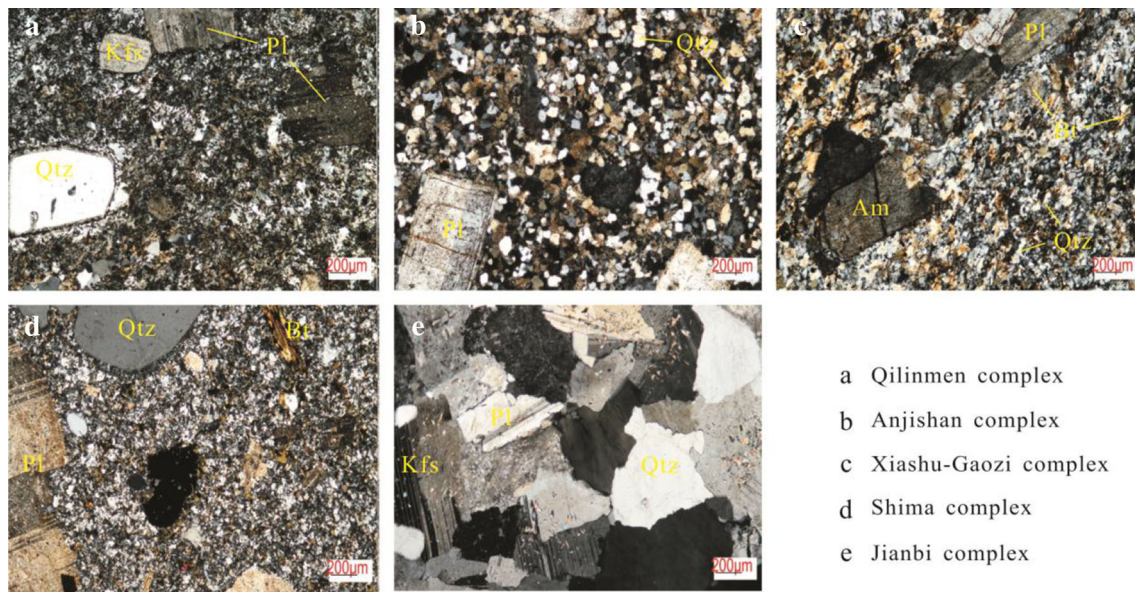
The Ningzhen region is located along the eastern boundary of the North China Craton at the northern margin of the Yangtze Block, where Yanshanian magmatism is extensively developed (Fig. 1a). The stratigraphy in this region is divided into three units (Bureau of Geology and Mineral Exploration of Jiangsu Province 1989): early and middle Proterozoic to Sinian basement strata that have undergone slight migmatization and low-grade metamorphism, Sinian to Triassic sedimentary cover comprising a marine to terrestrial facies succession, and Jurassic to Cretaceous superimposed cover comprising a thick terrestrial succession of red clastic and volcanic intrusive rocks. The structural framework is dominated by folds and faults and is comparatively

complex in this region. The compound fold structure consists of a series of parallel folds with E–W axes and has an E–W orientation. The fault structures are characterized mainly by E–W thrust faults on both sides of the anticline and include NW- and NE-trending conjugate shear faults. Magmatic activity in the Ningzhen region occurred mainly in the Yanshanian followed by the Himalayan, which included only a small amount of basic magmatic activity. The regional magmatic activity in the Yanshanian was intense as is characterized by multi-stage and multi-period evolution. The intrusive rocks are located mainly along the fault zones and in the cores of the folds, and their lithology is mainly intermediate–acidic.

3 Samples and petrography

The Mesozoic intermediate–acidic intrusive complexes are extensively developed in the Ningzhen region (Fig. 1b). The Qilinmen complex covers an area of $\sim 14 \text{ km}^2$ trending NNW and dipping NEE. The main rock types in the Qilinmen complex are granite porphyry, diorite porphyrite, and quartz diorite porphyry. The granite porphyry samples, which were collected in Niutoushan at $32^\circ 03' 44.3'' \text{N}$ and $118^\circ 55' 42.0'' \text{E}$, have not undergone weathering. They contain a few melanocratic minerals and exhibit a porphyritic texture and blocky structure. The phenocryst composition is 15–20% plagioclase, 8–10% quartz, and 4–6% K-feldspar. The matrix has a granitic microstructure and consists of K-feldspar, plagioclase, quartz, and a small amount of biotite. The accessory minerals include zircon, magnetite, and apatite (Fig. 2a).

The Anjishan complex has been the subject of previous geochemical studies (Xu et al. 2001, 2002; Zeng et al. 2013). Its main rock types are granodiorite porphyry and



a Qilinmen complex
 b Anjishan complex
 c Xiashu-Gaozi complex
 d Shima complex
 e Jianbi complex

Fig. 2 Representative photomicrographs of the five intrusive rocks from the Ningzhen region. *Pl* plagioclase, *Kfs* potash feldspar, *Qtz* quartz, *Am* amphibole, *Bt* biotite

quartz diorite porphyrite. The studied granodiorite porphyry samples, situated at 32°06′19.4″N and 119°04′40.3″E, exhibit no weathering, and they have a porphyritic texture and blocky structure. The phenocrysts composition is 10–15% plagioclase, 5–8% hornblende, 2–5% K-feldspar, and 1–3% quartz. The matrix has a granitic microstructure and consists of K-feldspar, plagioclase, quartz, and a small amount of biotite. The accessory minerals include sphene, zircon, and apatite (Fig. 2b).

The main rock types in the Xiashu–Gaozi complex include quartz diorite porphyrite, granodiorite, monzonitic granite, quartz diorite, and quartz monzonite. The quartz diorite porphyrite samples, situated at 32°09′42.9″N and 119°07′10.7″E, exhibit slight alteration and have a porphyritic texture and blocky structure. The phenocrysts are dominated by plagioclase, followed by hornblende, and biotite. The matrix has an anhedral to subhedral structure and consists of quartz, hornblende, biotite, and a small amount of pyroxene. The accessory minerals include apatite, sphene, and magnetite (Fig. 2c).

The Shima complex is located to the southwest of Zhenjiang City and covers an area of ~ 34 km²; its main rock types are granodiorite porphyry, diorite porphyrite, and syenite granite. The granodiorite porphyry samples, situated at 32°08′14.9″N and 119°17′40.7″E, exhibit slight alteration and have a porphyritic texture and blocky structure. The phenocrysts are dominated by plagioclase and K-feldspar, followed by hornblende, and biotite. The matrix has a crystal microstructure and consists of K-feldspar, plagioclase, quartz, and small amounts of

hornblende and biotite. The accessory minerals include apatite, sphene, zircon, and magnetite (Fig. 2d).

The Jianbi complex trends E–W and is located in Jianbi Town, Zhenjiang City. The bedrock area is ~ 46 km². The main rock types in the Jianbi complex are monzonitic granite, quartz diorite porphyry, and quartz monzonite porphyry. The monzonitic granite is genetically related to a W–Mo deposit. The samples, situated at 32°10′38.3″N and 119°33′06.4″E, exhibit no weathering and have a hypidiomorphic granular texture and blocky structure. The main minerals are 30–40% plagioclase, 25–30% K-feldspar, and 15–20% quartz. The melanocratic minerals are hornblende and biotite, each at 5%. The accessory minerals include sphene, zircon, and apatite, with a total content of ~ 5% (Fig. 2e).

4 Analytical methods

The zircon crystals were separated by using the conventional heavy liquid and magnetic techniques described in detail by Dubé et al. (1996). The original rock samples were crushed into powder. Then, heavy mineral separation was performed using an electromagnetic separator, and a binocular microscope was used to select zircon grains with good crystallinity and transparency (Romeo et al. 2006). The zircons were set in an epoxy mount, which was polished and buffed. Prior to LA–ICP–MS zircon U–Pb isotope analysis, the morphology and internal structures of these zircons were studied using a binocular microscope and cathodo luminescence (CL) imaging to determine

appropriate points for the analysis. The CL observation and photography as well as LA–ICP–MS zircon U–Pb isotope analysis were conducted at the State Key Laboratory of Ore Deposit Geochemistry (SKLOGD), Institute of Geochemistry, Chinese Academy of Sciences. Laser sampling was performed by using a *GeoLas Pro* 193 nm ArF excimer laser. An Agilent 7500 × ICP–MS instrument was used to acquire ion-signal intensities. He was applied as a carrier gas and was mixed with Argon via a T-connector before entering the ICP–MS. Each analysis incorporated a background acquisition of approximately 30 s gas blank followed by 60 s of data acquisition from the sample. Off-line selection and integration of background and analyte signals, time-drift correction, and quantitative calibration for trace element analyses and U–Pb dating were performed by using ICPMSDataCal software (Liu et al. 2008, 2010a, b). Zircon 91500 was used as the external standard for U–Pb dating and was analyzed twice every six to eight analyses (i.e., two zircon 91500 + six–eight samples + two zircon 91500). Uncertainty of the preferred values for the external standard 91500 was propagated to the final results of the samples. Concordia diagrams and weighted mean calculations were developed by using the Isoplot program (Ludwig 2003). Because $^{207}\text{Pb}/^{206}\text{Pb}$ is sensitive to the common Pb corrections, the $^{206}\text{Pb}/^{238}\text{U}$ age is generally used for rocks younger than about 1000 Ma (Black et al. 2003). No common Pb correction was applied to the samples owing to the very low ^{204}Pb counts and its poor analytical precision. The trace amount of common Pb did not affect the $^{206}\text{Pb}/^{238}\text{U}$ ages. Therefore, $^{206}\text{Pb}/^{238}\text{U}$ ages, which are precise and stable, were used to calculate the crystallization ages for the samples.

Fresh parts of all original rock samples were carefully selected to avoid the weathered sections, and the samples were then crushed to 200-mesh size. The major element abundances in whole rocks were determined on fused glass discs by using an AXIOS-PW4400 X-ray fluorescence (XRF) instrument at SKLOGD, Institute of Geochemistry, Chinese Academy of Sciences. The accuracy was monitored by using Chinese national standard GSR-3. The accuracy for major elements was better than $\pm 2\%$. The loss-on-ignition (LOI) was determined by the weight loss of a powdered sample after 1 h at 1000 °C (Sun et al. 2017a, b, c).

The trace element concentrations were analyzed using a Perkin-Elmer Sciex Elan DRC-e quadrupole ICP–MS at SKLOGD. For each sample, 50 mg of powder was dissolved using a mixture of HF and HNO₃ in a Teflon bomb for 48 h at 190 °C. Rh was used to monitor signal drift during data acquisition. International standards GBPG-1 and OU-6 and Chinese national standards GSR-1 and GSR-3 were used to monitor accuracy. The difference between

our results and the recommended values for the standards was generally better than $\pm 10\%$ (Sun et al. 2017a, b, c).

5 Results

The results of LA–ICP–MS zircon U–Pb dating of the five typical complexes from the Ningzhen region, including common Pb correction, are shown in Table 1. The errors for each data analysis point, also listed in Table 1, were all 1σ . The CL images are shown in Fig. 3, and the concordia plots are shown in Fig. 4.

The zircon grains from the Qilinmen granite porphyry are mostly large, long-columnar, and idiomorphic with lengths of ~ 110 – $200\ \mu\text{m}$ and widths of ~ 50 – $80\ \mu\text{m}$. Their internal structure was largely uniform and clear and showed well-developed oscillatory zoning, which is characteristic of magmatic zircons (Fig. 3a). The contents of Th and U were high, at 338–1187 ppm and 447–1482 ppm, respectively. The ratio of Th/U ranged between 0.40 and 0.89 (Table 1), slightly larger than 0.50, with an average of 0.64 ($n = 15$). Positive correlation is present between the Th and U, which is also consistent with the general characteristics of magmatic zircons (Hoskin and Black 2000). The dates of 15 points were in agreement with each other, showing no large age fluctuations. This indicates that the U–Th–Pb isotopic system of the zircons was not affected by later magmatic activity, tectonic activity, or metamorphism and that the system was closed. The 15 data points were clustered in the concordia plots (Fig. 4a), and the weighted average age was $122.0 \pm 1.0\ \text{Ma}$ ($n = 15$, MSWD = 0.15), which dates the emplacement age of the Qilinmen complexes to the Early Cretaceous.

The zircon grains from the Anjishan granodiorite porphyry were mostly large, long-columnar, and idiomorphic, although a few were incomplete; their lengths and widths were ~ 130 – $190\ \mu\text{m}$ and ~ 40 – $70\ \mu\text{m}$. Their internal structure was largely uniform and clear and showed well-developed oscillatory zoning, which is a characteristic of magmatic zircons (Fig. 3b). The contents of Th and U were high, at 977–3530 ppm and 1006–2043 ppm, respectively. The ratio of Th/U was 0.97–1.73 (Table 1) with an average of 1.32 ($n = 15$) and was typically greater than 0.50. A positive correlation exists between the Th and U, which is also consistent with the general characteristics of magmatic zircons. The dates of 15 points were in agreement with each other, with no large fluctuations in age. This indicates that the U–Th–Pb isotopic system of the zircons was not affected by later magmatic activity, tectonic activity, or metamorphism and that the system was closed. The 15 data points were clustered in the concordia plots (Fig. 4b), and the weighted average age was $106.1 \pm 0.8\ \text{Ma}$ ($n = 15$,

Table 1 LA–ICP–MS zircon U–Pb ages of the five complexes in the Ningzhen region

Spot	Concentrations (ppm)			Th/U	U–Th–Pb isotopic ratios					
	Pb _{total}	Th	U		²⁰⁷ Pb/ ²⁰⁶ Pb	1σ	²⁰⁷ Pb/ ²³⁵ U	1σ	²⁰⁶ Pb/ ²³⁸ U	1σ
<i>QLM-2 (granite porphyry)</i>										
QLM-2-1	47.7	476	865	0.55	0.0531	0.0022	0.1419	0.0063	0.0193	0.0003
QLM-2-2	66.6	693	986	0.70	0.0449	0.0017	0.1191	0.0046	0.0191	0.0002
QLM-2-3	45.5	413	842	0.49	0.0517	0.0021	0.1377	0.0058	0.0192	0.0003
QLM-2-4	108.1	1187	1482	0.80	0.0471	0.0018	0.1243	0.0047	0.0191	0.0003
QLM-2-5	51.3	509	974	0.52	0.0490	0.0021	0.1297	0.0055	0.0191	0.0002
QLM-2-6	76.1	604	1064	0.57	0.0527	0.0020	0.1105	0.0039	0.0153	0.0002
QLM-2-7	80.0	841	1267	0.66	0.0496	0.0017	0.1297	0.0043	0.0190	0.0002
QLM-2-8	74.0	765	1062	0.72	0.0557	0.0021	0.1461	0.0055	0.0190	0.0003
QLM-2-9	42.5	361	912	0.40	0.0540	0.0022	0.1415	0.0056	0.0191	0.0002
QLM-2-10	97.9	1034	1443	0.72	0.0490	0.0017	0.1301	0.0045	0.0192	0.0002
QLM-2-11	30.7	399	447	0.89	0.0720	0.0030	0.1898	0.0084	0.0191	0.0003
QLM-2-12	65.2	560	1117	0.50	0.0611	0.0032	0.1691	0.0082	0.0202	0.0003
QLM-2-13	51.4	338	768	0.44	0.0829	0.0044	0.2268	0.0124	0.0195	0.0003
QLM-2-14	50.5	532	739	0.72	0.0511	0.0022	0.1355	0.0058	0.0192	0.0003
QLM-2-15	42.1	405	756	0.54	0.0529	0.0021	0.1418	0.0061	0.0192	0.0003
<i>AJS-7 (granodiorite porphyry)</i>										
AJS-7-1	212.8	2280	1535	1.49	0.0517	0.0031	0.1167	0.0070	0.0165	0.0002
AJS-7-2	173.4	1805	1387	1.30	0.0593	0.0032	0.1341	0.0072	0.0165	0.0003
AJS-7-3	96.6	977	1006	0.97	0.0503	0.0036	0.1138	0.0079	0.0164	0.0003
AJS-7-4	180.7	1852	1606	1.15	0.0528	0.0027	0.1195	0.0060	0.0165	0.0003
AJS-7-5	205.1	2108	1529	1.38	0.0490	0.0026	0.1104	0.0056	0.0165	0.0003
AJS-7-6	157.3	1601	1209	1.32	0.0535	0.0033	0.1203	0.0072	0.0165	0.0003
AJS-7-7	147.4	1584	1247	1.27	0.0534	0.0032	0.1199	0.0068	0.0166	0.0003
AJS-7-8	168.2	1769	1354	1.31	0.0486	0.0025	0.1114	0.0059	0.0166	0.0002
AJS-7-9	199.4	2036	1567	1.30	0.0487	0.0025	0.1112	0.0059	0.0166	0.0002
AJS-7-10	169.7	1760	1423	1.24	0.0463	0.0026	0.1061	0.0060	0.0165	0.0003
AJS-7-11	145.8	1528	1244	1.23	0.0536	0.0036	0.1197	0.0076	0.0166	0.0003
AJS-7-12	135.8	1410	1172	1.20	0.0476	0.0027	0.1075	0.0059	0.0165	0.0003
AJS-7-13	237.2	2560	1794	1.43	0.0491	0.0028	0.1107	0.0060	0.0165	0.0002
AJS-7-14	329.9	3530	2043	1.73	0.0469	0.0022	0.1062	0.0050	0.0165	0.0002
AJS-7-15	239.0	2658	1730	1.54	0.0539	0.0027	0.1225	0.0058	0.0166	0.0002
<i>XG-6 (quartz diorite porphyrite)</i>										
XG-6-1	18.4	493	460	1.07	0.0735	0.0064	0.1573	0.0105	0.0169	0.0005
XG-6-2	18.2	384	350	1.10	0.0702	0.0066	0.1628	0.0198	0.0168	0.0004
XG-6-3	10.9	631	497	1.27	0.0598	0.0059	0.1614	0.0117	0.0172	0.0003
XG-6-4	14.6	683	578	1.18	0.0689	0.0048	0.1540	0.0122	0.0170	0.0003
XG-6-5	14.1	724	608	1.19	0.0597	0.0047	0.1626	0.0109	0.0171	0.0004
XG-6-6	13.7	492	471	1.04	0.0683	0.0070	0.1568	0.0134	0.0172	0.0002
XG-6-7	11.6	573	495	1.16	0.0614	0.0065	0.1617	0.0163	0.0165	0.0003
XG-6-8	11.8	465	513	0.91	0.0639	0.0063	0.1624	0.0117	0.0167	0.0004
XG-6-9	13.1	476	466	1.02	0.0707	0.0053	0.1586	0.0156	0.0165	0.0003
XG-6-10	17.5	671	580	1.16	0.0756	0.0060	0.1570	0.0118	0.0174	0.0003
XG-6-11	14.4	602	585	1.03	0.0677	0.0058	0.1547	0.0115	0.0167	0.0002
XG-6-12	14.0	487	461	1.06	0.0711	0.0050	0.1592	0.0102	0.0171	0.0005
XG-6-13	15.3	747	613	1.22	0.0690	0.0065	0.1562	0.0120	0.0169	0.0004
XG-6-14	15.8	480	487	0.99	0.0547	0.0052	0.1625	0.0113	0.0168	0.0004

Table 1 continued

Spot	Concentrations (ppm)			Th/U	U–Th–Pb isotopic ratios					
	Pb _{total}	Th	U		²⁰⁷ Pb/ ²⁰⁶ Pb	1σ	²⁰⁷ Pb/ ²³⁵ U	1σ	²⁰⁶ Pb/ ²³⁸ U	1σ
XG-6-15	12.8	643	706	0.91	0.0754	0.0053	0.1582	0.0115	0.0167	0.0002
<i>SM-1 (granodiorite porphyry)</i>										
SM-1-1	6.7	410	291	1.41	0.0623	0.0101	0.1272	0.0086	0.0169	0.0006
SM-1-2	7.2	394	288	1.37	0.0632	0.0087	0.1185	0.0113	0.0164	0.0004
SM-1-3	16.0	707	592	1.19	0.0502	0.0040	0.1179	0.0077	0.0153	0.0003
SM-1-4	12.2	487	526	0.93	0.0540	0.0035	0.1174	0.0069	0.0158	0.0003
SM-1-5	18.7	323	566	0.57	0.1113	0.0063	1.2370	0.0990	0.0632	0.0045
SM-1-6	9.3	387	415	0.93	0.0599	0.0041	0.1303	0.0085	0.0165	0.0003
SM-1-7	9.8	465	450	1.03	0.0582	0.0033	0.1205	0.0080	0.0158	0.0002
SM-1-8	10.4	540	553	0.98	0.0544	0.0039	0.1140	0.0073	0.0162	0.0002
SM-1-9	8.2	576	512	1.13	0.0610	0.0054	0.1244	0.0061	0.0164	0.0004
SM-1-10	13.5	646	587	1.10	0.0538	0.0033	0.1162	0.0071	0.0161	0.0003
SM-1-11	12.1	539	504	1.07	0.0565	0.0067	0.0991	0.0076	0.0157	0.0002
SM-1-12	8.8	434	436	1.00	0.0721	0.0081	0.0998	0.0092	0.0163	0.0003
SM-1-13	16.4	458	443	1.03	0.0855	0.0072	0.1224	0.0066	0.0163	0.0004
SM-1-14	7.8	601	582	1.03	0.0708	0.0047	0.1315	0.0058	0.0168	0.0005
SM-1-15	13.5	453	419	1.08	0.0572	0.0030	0.1246	0.0065	0.0160	0.0003
<i>JB-3 (monzonitic granite)</i>										
JB-3-1	29.5	402	379	1.06	0.0576	0.0036	0.1195	0.0072	0.0150	0.0003
JB-3-2	8.7	121	89	1.37	0.0814	0.0070	0.1673	0.0130	0.0151	0.0004
JB-3-3	20.2	301	143	2.11	0.0810	0.0088	0.1612	0.0154	0.0151	0.0004
JB-3-4	10.2	145	112	1.30	0.0815	0.0074	0.1507	0.0115	0.0151	0.0004
JB-3-5	10.1	123	99	1.25	0.0827	0.0077	0.1601	0.0134	0.0151	0.0004
JB-3-6	14.6	174	123	1.41	0.0864	0.0063	0.1812	0.0136	0.0151	0.0004
JB-3-7	23.6	355	261	1.36	0.0605	0.0055	0.1228	0.0095	0.0154	0.0003
JB-3-8	13.3	181	126	1.43	0.0778	0.0072	0.1571	0.0130	0.0150	0.0004
JB-3-9	19.6	260	120	2.17	0.1151	0.0093	0.2259	0.0152	0.0152	0.0004
JB-3-10	13.8	184	126	1.46	0.0842	0.0069	0.1670	0.0120	0.0151	0.0004
JB-3-11	18.3	262	161	1.63	0.0774	0.0061	0.1567	0.0119	0.0151	0.0003
JB-3-12	14.7	208	134	1.55	0.0845	0.0080	0.1700	0.0152	0.0151	0.0003
JB-3-13	10.8	130	201	0.65	0.0686	0.0049	0.1450	0.0099	0.0155	0.0003
JB-3-14	8.5	114	93	1.23	0.0790	0.0072	0.1567	0.0121	0.0151	0.0004
JB-3-15	10.9	155	96	1.61	0.1035	0.0117	0.2084	0.0199	0.0154	0.0005
<i>QLM-2 (granite porphyry)</i>										
QLM-2-1	Ages (Ma)									
	²⁰⁷ Pb/ ²⁰⁶ Pb			1σ	²⁰⁷ Pb/ ²³⁵ U	1σ	²⁰⁶ Pb/ ²³⁸ U	1σ		
QLM-2-1	332			99	135	6	123			2
QLM-2-2	253			86	114	4	122			1
QLM-2-3	272			93	131	5	122			2
QLM-2-4	54			89	119	4	122			2
QLM-2-5	146			100	124	5	122			1
QLM-2-6	317			117	116	4	127			1
QLM-2-7	176			80	124	4	121			2
QLM-2-8	439			83	138	5	121			2
QLM-2-9	372			89	134	5	122			1
QLM-2-10	146			86	124	4	122			1

Table 1 continued

Spot	Ages (Ma)					
	$^{207}\text{Pb}/^{206}\text{Pb}$	1 σ	$^{207}\text{Pb}/^{235}\text{U}$	1 σ	$^{206}\text{Pb}/^{238}\text{U}$	1 σ
QLM-2-11	987	117	176	7	122	2
QLM-2-12	643	114	159	7	129	2
QLM-2-13	1278	104	208	10	125	2
QLM-2-14	243	98	129	5	122	2
QLM-2-15	324	89	135	5	123	2
<i>AJS-7 (granodiorite porphyry)</i>						
AJS-7-1	272	139	112	6	105	1
AJS-7-2	576	123	128	6	105	2
AJS-7-3	209	163	109	7	105	2
AJS-7-4	320	117	115	5	105	2
AJS-7-5	146	158	106	5	106	2
AJS-7-6	350	137	115	7	105	2
AJS-7-7	346	135	115	6	106	2
AJS-7-8	128	– 72	107	5	106	2
AJS-7-9	200	120	107	5	106	2
AJS-7-10	9	133	102	6	106	2
AJS-7-11	354	152	115	7	106	2
AJS-7-12	80	130	104	5	105	2
AJS-7-13	154	135	107	5	106	1
AJS-7-14	43	107	102	5	106	1
AJS-7-15	369	111	117	5	106	1
<i>XG-6 (quartz diorite porphyrite)</i>						
XG-6-1	251	118	145	8	111	2
XG-6-2	429	183	128	8	113	3
XG-6-3	243	129	109	6	109	2
XG-6-4	192	93	112	4	109	2
XG-6-5	288	102	116	12	106	3
XG-6-6	267	133	103	5	107	2
XG-6-7	262	135	127	8	108	2
XG-6-8	401	148	152	10	100	3
XG-6-9	249	177	107	8	110	2
XG-6-10	354	136	162	10	111	2
XG-6-11	319	107	130	11	108	2
XG-6-12	323	105	146	9	109	3
XG-6-13	297	170	120	8	107	2
XG-6-14	368	221	167	11	112	2
XG-6-15	272	113	141	9	109	2
<i>SM-1 (granodiorite porphyry)</i>						
SM-1-1	632	316	121	17	102	2
SM-1-2	720	185	138	10	106	3
SM-1-3	710	237	114	7	103	2
SM-1-4	848	280	143	12	103	1
SM-1-5	1821	77	772	47	394	27
SM-1-6	547	213	123	7	105	2
SM-1-7	627	288	119	8	100	2
SM-1-8	395	154	112	8	97	3
SM-1-9	646	166	137	10	104	2

Table 1 continued

Spot	Ages (Ma)					
	$^{207}\text{Pb}/^{206}\text{Pb}$	1 σ	$^{207}\text{Pb}/^{235}\text{U}$	1 σ	$^{206}\text{Pb}/^{238}\text{U}$	1 σ
SM-1-10	820	181	105	6	103	1
SM-1-11	694	175	148	9	102	1
SM-1-12	725	338	172	14	113	4
SM-1-13	887	149	186	15	101	3
SM-1-14	680	254	183	8	96	5
SM-1-15	788	174	110	6	105	2
<i>JB-3 (monzonitic granite)</i>						
JB-3-1	522	135	115	7	96	2
JB-3-2	1231	169	157	11	97	3
JB-3-3	1221	216	152	13	97	2
JB-3-4	1235	178	143	10	97	3
JB-3-5	1261	151	151	12	97	3
JB-3-6	1346	143	169	12	97	2
JB-3-7	620	196	118	9	99	2
JB-3-8	1143	185	148	11	96	3
JB-3-9	1881	146	207	13	97	2
JB-3-10	1298	161	157	10	97	3
JB-3-11	1131	158	148	10	97	2
JB-3-12	1306	184	159	13	97	2
JB-3-13	887	149	137	9	99	2
JB-3-14	1172	177	148	11	97	3
JB-3-15	1687	209	192	17	98	3

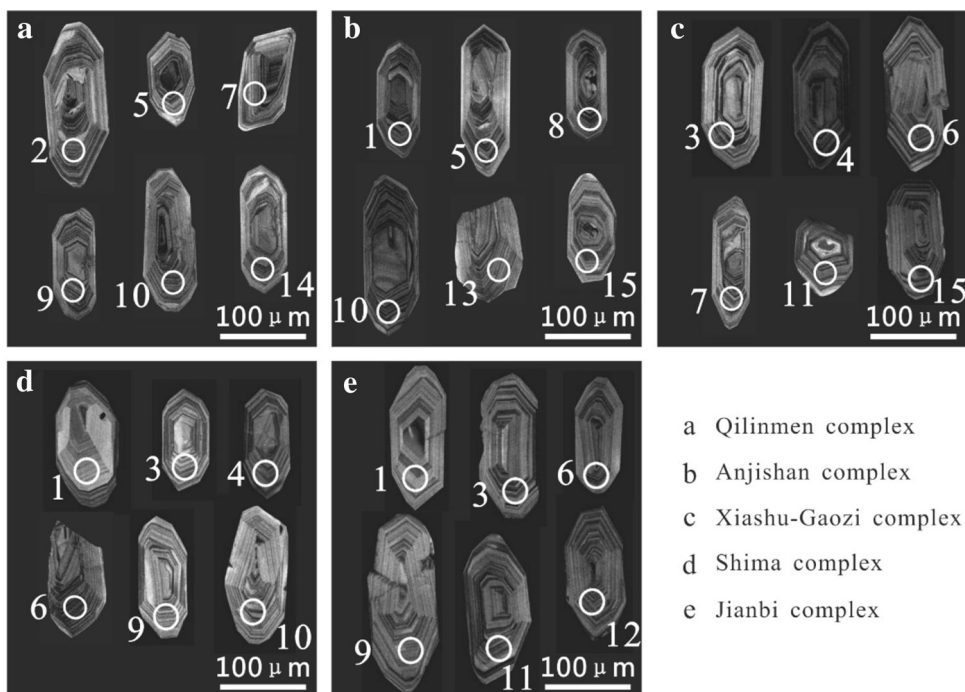
MSWD = 0.90), which dates the emplacement age of the Anjishan complexes to the Early Cretaceous.

The zircon grains from the Xiashu–Gaozi quartz diorite porphyrite were mostly large, long-columnar, and idiomorphic, although a few were incomplete; their lengths and widths were ~ 100 – $180 \mu\text{m}$ and ~ 40 – $80 \mu\text{m}$, respectively. Their internal structure was uniform and clear and showed well-developed oscillatory zoning, which is characteristic of magmatic zircons (Fig. 3c). The contents of Th and U were high, at 384–747 ppm and 350–706 ppm, respectively. The ratio of Th/U ranged between 0.91 and 1.27 with an average of 1.09 ($n = 15$) and was typically greater than 0.50 (Table 1). A positive correlation was present between the Th and U, which was also consistent with the general characteristics of magmatic zircons. The dates of 15 points were in agreement with each other, with no large fluctuations in age. This indicates that the U–Th–Pb isotopic system of the zircons was not affected by later magmatic activity, tectonic activity, or metamorphism and that the system was closed. The 15 data points were clustered in the concordia plots (Fig. 4c), and the weighted

average age was $108.7 \pm 1.4 \text{ Ma}$ ($n = 15$, MSWD = 0.45), which dates the emplacement age of the Xiashu–Gaozi complexes to the Early Cretaceous.

The zircon grains from the Shima granodiorite porphyry were large, long-columnar, and idiomorphic, although a few were incomplete and asymmetric; their lengths and widths were ~ 120 – $160 \mu\text{m}$ and ~ 50 – $80 \mu\text{m}$, respectively. Their internal structure was largely uniform and clear and showed well-developed oscillatory zoning, which is characteristic of magmatic zircons (Fig. 3d). The contents of the Th and U are 387–707 ppm and 288–592 ppm, respectively. The ratio of Th/U ranged between 0.93 and 1.41 (Table 1) with an average of 1.09 ($n = 14$) and was typically greater than 0.50. A positive correlation is present between the Th and U, which is also consistent with the general characteristics of magmatic zircons. At 394 Ma, the age of one zircon was obviously older than that of the other fourteen. We speculate that the early zircon crystallization was inherited by early magmatic activity; therefore, the age of this zircon was eliminated when calculating the diagenetic age. In this case, the 14 $^{206}\text{Pb}/^{238}\text{U}$ dates

Fig. 3 CL images of selected zircons from the five intrusive rocks



- a Qilinmen complex
- b Anjishan complex
- c Xiashu-Gaozi complex
- d Shima complex
- e Jianbi complex

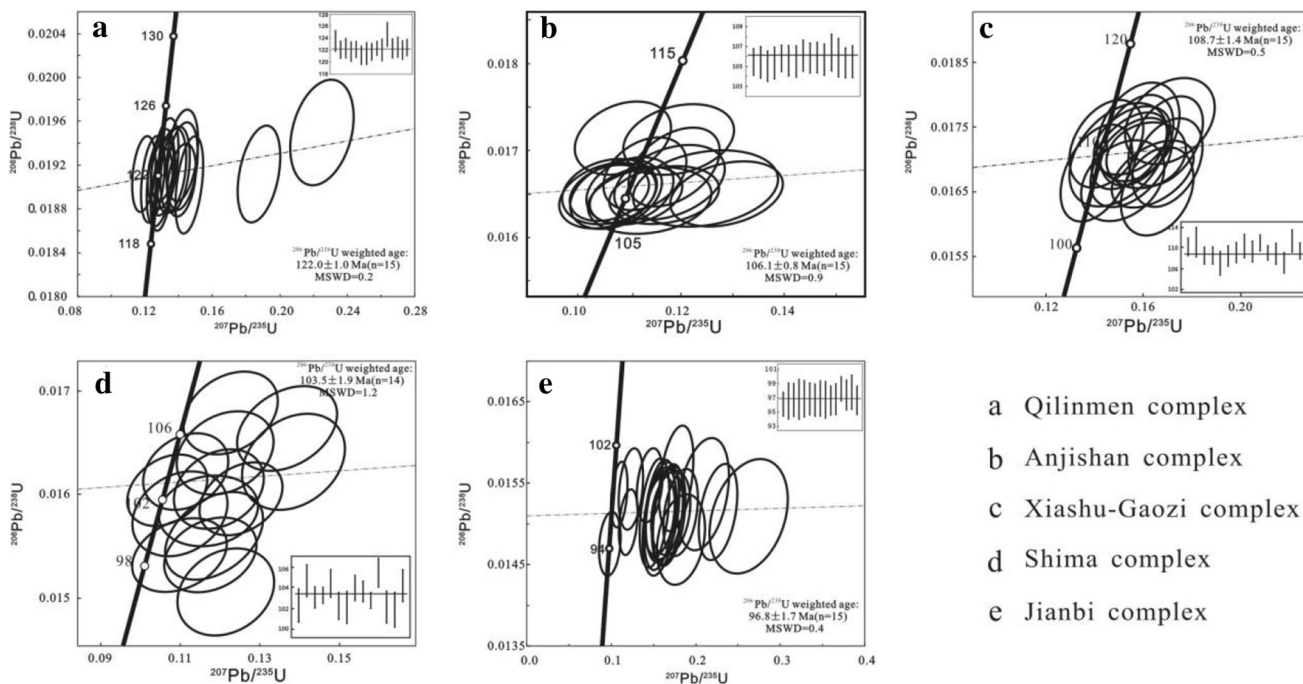


Fig. 4 Zircon LA-ICP-MS U-Pb concordia plots for the five complexes

obtained by the LA-ICP-MS method were distributed on or near the U/Pb harmonic line in the concordia plots (Fig. 4d), and the weighted average age was 103.5 ± 1.9 Ma ($n = 14$, $MSWD = 1.20$), which dates the emplacement age of the Shima complexes to the Early Cretaceous. The scattered $^{207}\text{Pb}/^{235}\text{U}$ numerical values in

the sample concordia plots may be attributed to the inaccuracy of the ^{207}Pb count.

The zircons from the Jianbi monzonitic granite were long-columnar, euhedral, and subhedral, exhibiting lengths of $\sim 140\text{--}200\ \mu\text{m}$ and widths of $\sim 50\text{--}90\ \mu\text{m}$. Their internal structure was relatively uniform and clear and showed well-developed oscillatory zoning, which is

characteristic of magmatic zircons (Fig. 3e). The contents of Th and U are 114–402 ppm and 89–379 ppm, respectively. The ratio of Th/U ranges between 0.65 and 2.17 (Table 1) with an average of 1.44 ($n = 15$) and was typically greater than 0.50. A positive correlation exists between the Th and U, which is also consistent with the general characteristics of magmatic zircons. These results indicate that the zircons from the Jianbi complexes are magmatic in origin. The $^{15} \text{ }^{206}\text{Pb}/^{238}\text{U}$ dates obtained by the LA-ICP-MS method were distributed on or near the U/Pb harmonic line in the concordia plot (Fig. 4e), and the weighted average age was 96.8 ± 1.7 Ma ($n = 15$, MSWD = 0.40), which suggests that the Jianbi complexes were emplaced in the Early Cretaceous.

6 Litho geochemistry

6.1 Major element geochemical characteristics

In this paper, litho geochemical research was conducted on 31 representative samples; their major (wt%) and trace element (ppm) analysis results and relevant parameters are listed in Table 2.

As shown in Table 2 and Fig. 5, the intermediate–acidic intrusive complexes had high SiO_2 and relatively high MgO contents at maximum values of 73.40 and 2.25 wt%, respectively, and displayed significant positive Sr anomalies and negative Ta, Nb and Ti anomalies, resembling those of adakitic rocks (Martin 1999; Xu et al. 2002). The total alkali ($\text{K}_2\text{O} + \text{Na}_2\text{O}$) content was generally high, ranging from 6.49 to 8.68 wt%, with an average of 7.62 wt%. In the K_2O versus SiO_2 major element diagram (Fig. 5a), most of the intermediate–acidic rock samples plotted within the high-K calc-alkaline series, with a few situated within the calc-alkaline series. In the MgO versus SiO_2 major element diagram (Fig. 5b), most samples of Anjishan, Xiashu–Gaozi, and Shima fell in the overlap region between subducted oceanic slab-derived adakites and thickened lower crust-derived adakites. Moreover, most samples of Qilinmen and Jianbi fell in the region of metabasaltic and eclogite experimental melts. As illustrated in Harker diagrams (Fig. 6), each oxide shows a good correlation with SiO_2 . The SiO_2 is positively correlated with K_2O ; however, it is negatively correlated with Na_2O , TiO_2 , Al_2O_3 , FeO^{T} , MgO, CaO, and P_2O_5 .

6.2 Trace element geochemical characteristics

The REE content was generally high in the intermediate–acidic intrusive complexes of the Ningzhen region; the ΣREE ranged from 70.68 to 184.59 ppm with an average of 148.60 ppm. The chondrite-normalized REE patterns of

the five complexes were essentially similar. The REE patterns also exhibited right-inclined curves. They are characterized by enrichment in light rare earth elements (LREE) and depletion in heavy rare earth elements (HREE), showing high $(\text{La}/\text{Yb})_{\text{N}}$ ratios of 15.02–37.28 and slightly negative Eu anomalies (Fig. 7a, Table 2). These characteristics indicate that the magmatic evolution process in the Ningzhen region was consistent. The numerical values of δEu in the five complexes ranged between 0.69 and 1.13, with an average of 0.90; the majority show slightly negative Eu anomalies, and the minority show slightly positive Eu anomalies. The positive Eu anomalies suggest that no plagioclase fractional crystallization occurred during the formation process of the intrusive rocks or that the crystallization time was short. In addition, the $(\text{La}/\text{Yb})_{\text{N}}$ ratio in the intermediate–acidic intrusive complexes ranged from 15.02 to 37.28, which is generally higher than that in both the lower crust and upper crust, at $(\text{La}/\text{Yb})_{\text{N}} = 5.30$ and 15.50, respectively (Rudnick and Gao 2003). This suggests that the complexes in the Ningzhen region experienced intense REE differentiation.

The primitive-mantle-normalized trace element patterns (Fig. 7b) show that all five complexes are enriched in LILE, including Rb, Ba, and K, and are strongly depleted in HFSE, including Nb, Ta, P, Zr, and Ti. Therefore, the trace element curve gradually decreases toward the right. The trace element geochemical characteristics show that fractional crystallization in the magmatic evolution process may have involved apatite, Ti-rich minerals, and hornblende. This result corroborates the REE analysis results. In the $(\text{La}/\text{Yb})_{\text{N}}-\delta\text{Eu}$ diagrams (Fig. 8), the samples all plot in the crust-mantle type field. The crust-mantle mixing (crust-mantle type) has been used by many researchers recently to study the genesis of granitoids (Castro et al. 1991; Liu and Li 2001; Nguyen and Kozo 2003; Chen et al. 2009). The genesis of granitoids has a close relationship with crust-mantle interaction. The granitoid components may be derived from the mantle as well as the crust. Moreover, it is believed that crust-mantle mixing in various degrees might form many types of granitoids. Granitic magma is formed by the mixing of crustal materials with mantle materials by subduction, detachment, underplating, mantle pluming, or other processes. The petrological, geochemical, isotopic, and geochronological characteristics of granitoids could be used to determine whether the genesis of a granitoid is related to crust-mantle interaction.

Table 2 Whole-rock geochemistry results including major (wt%) and trace element (ppm) compositions of the five complexes

Sample	Qiliminen complex									Anjishan complex									Xiashu-Gaozi complex				
	QLM-1	QLM-3	QLM-4	QLM-5	QLM-6	QLM-9	AJS-1	AJS-3	AJS-4	AJS-5	AJS-6	AJS-9	XG-1	XG-2	XG-3	XG-4							
	69.91	71.86	73.40	69.82	72.81	70.44	64.87	66.43	65.76	67.52	68.28	66.14	66.41	68.69	66.52	67.29							
SiO ₂	0.35	0.31	0.09	0.38	0.21	0.27	0.50	0.68	0.47	0.43	0.44	0.65	0.48	0.46	0.49	0.42							
TiO ₂	17.18	16.58	15.60	16.89	15.17	16.21	16.10	15.02	14.80	15.51	14.59	15.14	14.74	14.35	15.25	14.63							
Al ₂ O ₃	2.63	1.78	2.35	2.74	2.39	2.50	3.53	4.67	4.74	2.88	3.02	3.57	1.95	1.86	1.74	1.82							
FeO ^T	0.01	0.01	0.01	0.02	0.01	0.01	0.05	0.06	0.06	0.09	0.06	0.06	0.07	0.06	0.07	0.06							
MnO	0.11	0.12	0.09	0.39	0.10	0.23	2.08	2.25	1.96	1.50	2.01	2.17	2.02	1.80	1.82	1.78							
MgO	0.88	0.59	0.68	0.61	0.49	0.97	4.17	3.70	4.09	3.07	4.13	3.68	3.32	3.81	3.67	3.21							
CaO	3.88	3.52	3.50	4.13	4.02	3.80	4.36	3.97	4.13	4.28	4.02	4.12	3.99	3.75	3.89	4.07							
Na ₂ O	4.15	4.45	3.78	4.43	4.07	4.13	2.97	2.52	3.12	3.73	2.93	3.01	4.15	3.78	4.18	4.61							
K ₂ O	0.17	0.14	0.11	0.18	0.18	0.16	0.27	0.30	0.28	0.20	0.32	0.25	0.18	0.10	0.22	0.20							
P ₂ O ₅	0.72	0.64	0.41	0.39	0.55	1.28	1.10	0.41	0.57	0.78	0.21	1.22	2.68	1.34	2.13	1.91							
LOI	99.99	100.00	100.02	99.98	100.00	100.00	100.00	100.01	99.98	99.99	100.01	100.01	99.99	100.00	99.98	100.00							
total	8.03	7.97	7.28	8.56	8.09	7.93	7.33	6.49	7.25	8.01	6.95	7.13	8.14	7.53	8.07	8.68							
Na ₂ O + K ₂ O	12.04	13.09	78.71	113.54	85.78	102.10	47.27	51.31	35.25	42.30	45.68	49.76	90.39	127.02	87.84	76.43							
Rb	279.83	299.14	1723.62	1887.81	1814.27	1550.37	1853.52	1785.49	1957.02	1902.35	1859.21	1814.48	1417.92	1519.74	1763.61	1480.77							
Ba	10.30	9.87	9.73	10.53	10.36	9.61	10.91	14.80	8.26	8.92	10.36	12.32	12.66	11.10	10.38	12.17							
Th	1.19	0.82	0.78	1.13	0.97	0.88	2.72	3.86	2.41	2.83	2.57	3.96	1.43	1.93	1.86	1.78							
U	5.83	6.14	8.69	7.37	8.81	7.84	15.80	16.97	13.55	14.03	14.39	17.22	12.72	8.65	10.71	10.42							
Nb	0.64	0.78	0.86	0.71	0.82	0.84	1.32	1.36	1.25	1.54	1.20	1.39	1.07	0.84	1.06	0.93							
Ta	431.86	447.63	396.31	425.88	348.65	405.20	862.87	880.19	843.54	849.72	882.78	856.96	527.90	307.06	436.57	514.72							
Sr	136.66	135.91	122.12	118.40	136.24	121.03	80.78	82.74	79.66	80.47	81.34	80.19	160.10	183.49	175.34	176.03							
Zr	3.47	3.57	3.47	3.50	3.72	3.24	3.32	3.01	2.87	2.95	3.13	3.06	3.96	4.49	4.12	3.64							
Hf	8.75	5.45	10.39	9.77	6.82	11.30	10.56	12.14	8.09	9.72	11.33	9.25	10.11	9.68	9.97	10.23							
Y	29.44	18.68	23.03	27.42	31.15	28.84	38.61	47.82	37.26	42.84	40.36	43.58	35.41	44.42	47.28	34.20							
La	46.04	25.73	40.26	39.40	49.73	43.80	63.50	74.14	61.27	68.74	64.90	69.23	63.95	72.14	76.83	57.35							
Ce	6.31	3.87	4.56	5.08	5.81	4.89	6.83	7.96	6.52	7.78	7.02	7.56	6.90	7.60	7.73	5.93							
Pr	23.13	14.65	16.96	16.55	19.40	17.72	24.62	28.38	24.84	26.96	25.79	26.31	24.53	26.58	27.60	22.66							
Nd	3.51	2.32	2.87	2.66	3.58	3.34	4.32	4.52	4.10	4.28	4.30	4.43	3.64	3.75	4.23	3.34							
Sm	0.81	0.68	0.76	0.83	0.70	0.71	1.31	1.40	1.27	1.42	1.38	1.40	0.96	0.81	1.21	1.02							
Eu	2.59	1.69	2.40	2.08	2.33	1.98	3.57	3.76	3.50	3.64	3.55	3.71	2.97	3.06	3.14	2.79							
Gd	0.36	0.24	0.35	0.27	0.24	0.31	0.44	0.48	0.40	0.42	0.44	0.47	0.41	0.39	0.40	0.35							
Tb	1.72	1.16	1.89	1.53	1.81	1.73	1.96	2.29	1.89	2.01	2.10	2.14	2.05	1.91	2.55	1.87							
Dy	0.32	0.20	0.34	0.30	0.35	0.29	0.40	0.43	0.35	0.38	0.41	0.44	0.37	0.34	0.46	0.30							
Ho	0.87	0.58	0.98	0.64	1.01	0.85	0.93	1.02	0.86	0.97	0.85	0.95	1.04	0.98	1.23	0.97							
Er	0.16	0.12	0.18	0.15	0.19	0.21	0.11	0.13	0.12	0.12	0.10	0.12	0.18	0.17	0.27	0.17							
Tm																							

Table 2 continued

Sample	Qiliminen complex										Anjishan complex										Xiashu–Gaozi complex																								
	QLM-1	QLM-2	QLM-3	QLM-4	QLM-5	QLM-6	QLM-9	AJS-1	AJS-2	AJS-3	AJS-4	AJS-5	AJS-6	AJS-9	XG-1	XG-2	XG-3	XG-4	SM-3	SM-4	SM-6	SM-7	SM-10	SM-13	JB-1	JB-2	JB-5	JB-6	JB-8	JB-11	XG-5	XG-8	XG-10	SM-3	SM-4	SM-6	SM-7	SM-10	SM-13	JB-1	JB-2	JB-5	JB-6	JB-8	JB-11
Yb	0.99	0.67	1.10	0.72	0.77	0.88	0.90	0.92	0.94	0.88	0.86	0.88	0.88	0.88	1.05	1.00	1.09	0.97	66.32	67.19	66.21	64.74	67.34	68.10	69.18	68.69	71.85	70.93	71.36	72.49	68.64	65.54	66.37	66.32	67.19	66.21	64.74	67.34	68.10	69.18	68.69	71.85	70.93	71.36	72.49
TiO ₂	0.40	0.65	0.63	0.57	0.53	0.55	0.55	0.59	0.50	0.63	0.30	0.32	0.27	0.29	0.26	0.23	0.23	0.57	0.53	0.55	0.59	0.50	0.63	0.30	0.32	0.27	0.29	0.26	0.23	0.40	0.65	0.63	0.57	0.53	0.55	0.59	0.50	0.63	0.30	0.32	0.27	0.29	0.26	0.23	
Al ₂ O ₃	15.18	15.89	17.37	15.20	14.79	15.83	16.16	16.16	14.92	14.17	15.52	16.33	14.50	14.44	14.15	14.15	15.20	14.79	15.83	16.16	14.92	14.17	15.52	16.33	14.50	14.44	14.15	15.18	15.89	17.37	15.20	14.79	15.83	16.16	14.92	14.17	15.52	16.33	14.50	14.44	14.15				
FeO ^T	1.24	2.12	2.08	3.64	3.07	3.54	3.68	3.68	3.21	3.34	2.93	2.49	2.12	2.19	2.48	2.53	3.64	3.07	3.54	3.68	3.21	3.34	2.93	2.49	2.12	2.19	2.48	2.53	1.24	2.12	2.08	3.64	3.07	3.54	3.68	3.21	3.34	2.93	2.49	2.12	2.19	2.48	2.53		
MnO	0.06	0.09	0.08	0.07	0.07	0.05	0.06	0.06	0.06	0.08	0.03	0.04	0.04	0.02	0.02	0.02	0.07	0.07	0.05	0.06	0.06	0.08	0.03	0.04	0.04	0.02	0.02	0.02	0.06	0.09	0.08	0.07	0.07	0.05	0.06	0.06	0.08	0.03	0.04	0.04	0.02	0.02	0.02		
MgO	1.87	2.11	1.34	2.03	2.01	1.84	2.14	2.14	1.87	1.98	1.13	1.16	1.00	0.93	0.98	0.87	2.03	2.01	1.84	2.14	1.87	1.98	1.13	1.16	1.00	0.93	0.98	0.87	1.87	2.11	1.34	2.03	2.01	1.84	2.14	1.87	1.98	1.13	1.16	1.00	0.93	0.98	0.87		
CaO	3.39	3.53	3.47	3.35	3.24	3.15	3.49	3.49	3.64	3.68	1.72	1.81	1.70	1.79	1.84	1.80	3.35	3.24	3.15	3.49	3.64	3.68	1.72	1.81	1.70	1.79	1.84	1.80	3.39	3.53	3.47	3.35	3.24	3.15	3.49	3.64	3.68	1.72	1.81	1.70	1.79	1.84	1.80		
Na ₂ O	3.84	4.23	3.66	3.84	3.80	3.90	3.98	3.98	3.51	3.44	3.84	3.67	3.51	3.50	3.68	3.44	3.84	3.80	3.90	3.98	3.51	3.44	3.84	3.67	3.51	3.50	3.68	3.44	3.84	4.23	3.66	3.84	3.80	3.90	3.98	3.51	3.44	3.84	3.67	3.51	3.50	3.68	3.44		
K ₂ O	4.20	3.94	3.76	3.57	3.88	3.34	3.57	3.57	3.26	3.52	3.86	4.12	4.04	4.46	3.85	3.51	3.57	3.88	3.34	3.57	3.26	3.52	3.86	4.12	4.04	4.46	3.85	3.51	4.20	3.94	3.76	3.57	3.88	3.34	3.57	3.26	3.52	3.86	4.12	4.04	4.46	3.85	3.51		
P ₂ O ₅	0.17	0.22	0.31	0.21	0.17	0.20	0.18	0.18	0.24	0.23	0.15	0.15	0.11	0.12	0.14	0.09	0.21	0.17	0.20	0.18	0.24	0.23	0.15	0.15	0.11	0.12	0.14	0.09	0.17	0.22	0.31	0.21	0.17	0.20	0.18	0.18	0.24	0.23	0.15	0.15	0.11	0.12	0.14	0.09	
LOI	1.01	1.67	0.93	1.20	1.25	1.39	1.41	1.41	1.45	0.82	1.33	1.21	0.89	1.08	0.95	0.87	1.20	1.25	1.39	1.41	1.45	0.82	1.33	1.21	0.89	1.08	0.95	0.87	1.01	1.67	0.93	1.20	1.25	1.39	1.41	1.45	0.82	1.33	1.21	0.89	1.08	0.95	0.87		
total	100.00	99.99	100.00	100.00	100.00	100.00	100.00	100.00	100.00	99.99	99.99	99.99	100.00	100.00	100.00	100.00	100.00	100.00	100.00	100.00	100.00	99.99	99.99	99.99	100.00	100.00	100.00	100.00	100.00	99.99	100.00	100.00	100.00	100.00	100.00	100.00	100.00	99.99	99.99	100.00	100.00	100.00	100.00		
Na ₂ O + K ₂ O	8.04	8.17	7.42	7.41	7.68	7.24	7.55	7.55	6.77	6.96	7.70	7.79	7.55	7.96	7.53	6.95	7.41	7.68	7.24	7.55	6.77	6.96	7.70	7.79	7.55	7.96	7.53	6.95	8.04	8.17	7.42	7.41	7.68	7.24	7.55	6.77	6.96	7.70	7.79	7.55	7.96	7.53	6.95		
Rb	96.56	71.24	77.44	82.26	108.70	96.37	95.43	95.43	113.41	98.57	101.27	98.64	106.52	113.41	127.39	120.80	108.70	96.37	95.43	95.43	113.41	98.57	101.27	98.64	106.52	113.41	127.39	120.80	96.56	71.24	77.44	82.26	108.70	96.37	95.43	95.43	113.41	98.57	101.27	98.64	106.52	113.41	127.39	120.80	
Ba	1651.05	1346.53	1485.80	1507.12	1340.25	1381.95	1428.64	1428.64	1253.37	1463.50	1846.88	2122.39	1679.03	1506.17	2310.08	2225.63	1340.25	1381.95	1428.64	1428.64	1253.37	1463.50	1846.88	2122.39	1679.03	1506.17	2310.08	2225.63	1651.05	1346.53	1485.80	1507.12	1340.25	1381.95	1428.64	1428.64	1253.37	1463.50	1846.88	2122.39	1679.03	1506.17	2310.08	2225.63	
Th	11.50	7.93	8.66	9.71	12.89	12.35	11.73	11.73	13.62	12.67	7.85	7.55	7.62	9.77	10.25	6.11	12.89	12.35	11.73	11.73	13.62	12.67	7.85	7.55	7.62	9.77	10.25	6.11	11.50	7.93	8.66	9.71	12.89	12.35	11.73	11.73	13.62	12.67	7.85	7.55	7.62	9.77	10.25	6.11	
U	2.01	2.17	1.94	2.32	1.99	3.11	3.11	3.11	2.08	3.37	0.85	1.02	0.66	1.04	1.02	0.86	1.99	3.11	3.11	3.11	2.08	3.37	0.85	1.02	0.66	1.04	1.02	0.86	2.01	2.17	1.94	2.32	1.99	3.11	3.11	3.11	2.08	3.37	0.85	1.02	0.66	1.04	1.02	0.86	
Nb	12.15	13.67	14.15	14.37	15.76	16.72	15.39	15.39	15.10	14.03	8.32	7.41	9.34	6.11	8.97	10.14	15.76	16.72	15.39	15.39	15.10	14.03	8.32	7.41	9.34	6.11	8.97	10.14	12.15	13.67	14.15	14.37	15.76	16.72	15.39	15.39	15.10	14.03	8.32	7.41	9.34	6.11	8.97	10.14	
Ta	0.99	0.90	0.83	1.08	1.13	1.16	1.20	1.20	1.23	1.31	0.82	0.87	0.88	0.66	0.70	0.84	1.13	1.16	1.16	1.20	1.23	1.31	0.82	0.87	0.88	0.66	0.70	0.84	0.99	0.90	0.83	1.08	1.13	1.16	1.20	1.20	1.23	1.31	0.82	0.87	0.88	0.66	0.70	0.84	
Sr	401.83	617.55	534.25	712.37	574.63	532.70	581.01	581.01	487.28	554.92	387.11	434.99	332.54	338.56	427.67	564.23	574.63	532.70	581.01	581.01	487.28	554.92	387.11	434.99	332.54	338.56	427.67	564.23	401.83	617.55	534.25	712.37	574.63	532.70	581.01	581.01	487.28	554.92	387.11	434.99	332.54	338.56	427.67	564.23	
Zr	194.25	157.86	116.48	106.57	114.20	120.48	115.04	115.04	110.22	137.61	165.33	163.50	168.16	167.92	172.11	188.97	114.20	120.48	115.04	115.04	110.22	137.61	165.33	163.50	168.16	167.92	172.11	188.97	194.25	157.86	116.48	106.57	114.20	120.48	115.04	115.04	110.22	137.61	165.33	163.50	168.16	167.92	172.11	188.97	
Hf	4.03	3.49	2.64	3.28	2.85	3.02	2.79	2.79	2.85	3.60	4.40	4.46	4.38	4.04	4.73	4.92	2.85	3.02	3.02	2.79	2.85	3.60	4.40	4.46	4.38	4.04	4.73	4.92	4.03	3.49	2.64	3.28	2.85	3.02	2.79	2.79	2.85	3.60	4.40	4.46	4.38	4.04	4.73	4.92	
Y	9.86	14.54	13.23	12.75	10.47	11.36	11.04	11.04	9.87	10.23	9.28	8.93	10.33	10.75	13.18	12.82	10.47	11.36	11.04	11.04	9.87	10.23	9.28	8.93	10.33	10.75	13.18	12.82	9.86	14.54	13.23	12.75	10.47	11.36	11.04	11.04	9.87	10.23	9.28	8.93	10.33	10.75	13.18	12.82	
La	50.83	41.17	46.81	43.17	46.49	40.26	46.52	46.52	48.71	50.24	39.89	38.39	39.46	40.94	38.74	39.52	46.49	40.26	46.52	46.52	48.71	50.24	39.89	38.39	39.46	40.94	38.74	39.52	50.83	41.17	46.81	43.17	46.49	40.26	46.52	46.52	48.71	50.24	39.89	38.39	39.46	40.94	38.74	39.52	

Table 2 continued

Sample	Xiashu–Gaozi complex				Shima complex						Jianbi complex					
	XG-5	XG-8	XG-10		SM-3	SM-4	SM-6	SM-7	SM-10	SM-13	JB-1	JB-2	JB-5	JB-6	JB-8	JB-11
Ce	74.20	82.10	83.24		66.30	71.80	69.76	69.71	74.85	79.22	71.20	68.19	69.30	66.67	67.25	68.42
Pr	6.64	5.32	7.73		6.82	7.38	6.89	8.90	7.27	8.54	7.88	7.58	7.64	7.35	7.52	7.60
Nd	26.62	27.78	28.92		23.50	24.41	24.83	25.73	23.56	26.32	25.74	27.92	27.43	25.80	26.32	27.37
Sm	3.32	4.93	4.70		3.38	3.76	3.97	4.58	3.87	4.07	3.97	4.08	4.05	3.78	4.06	4.06
Eu	1.34	1.43	1.58		1.19	1.15	1.08	1.06	0.97	1.01	0.92	1.03	0.89	0.88	0.93	0.88
Gd	3.95	3.94	4.31		3.90	3.47	3.76	3.18	2.90	3.53	3.24	3.21	3.25	3.14	3.17	3.20
Tb	0.43	0.50	0.55		0.40	0.39	0.47	0.51	0.32	0.44	0.43	0.41	0.44	0.42	0.41	0.43
Dy	2.74	3.02	2.97		1.96	2.34	2.16	2.96	2.21	2.76	2.12	1.93	2.09	2.09	1.98	2.05
Ho	0.39	0.50	0.63		0.39	0.40	0.41	0.43	0.34	0.43	0.38	0.33	0.37	0.37	0.35	0.36
Er	1.13	1.39	1.52		1.24	1.21	1.15	1.33	1.10	1.20	0.91	0.89	1.00	1.02	0.92	0.97
Tm	0.26	0.18	0.21		0.14	0.17	0.18	0.17	0.16	0.16	0.17	0.15	0.17	0.18	0.15	0.16
Yb	1.18	1.23	1.28		0.93	1.13	1.03	1.04	0.98	0.99	0.96	0.85	0.97	1.05	0.99	0.94
Lu	0.15	0.18	0.14		0.18	0.18	0.15	0.17	0.15	0.15	0.14	0.12	0.14	0.15	0.13	0.14
∑REE	173.18	173.67	184.59		153.50	164.28	156.10	166.29	167.39	179.06	157.95	155.08	157.20	153.84	152.92	156.10
LREE/HREE	15.93	14.87	14.90		15.79	16.68	15.77	15.99	19.51	17.54	17.92	18.66	17.65	17.27	17.88	17.92
(La/Yb) _N	30.90	24.01	26.23		33.30	29.51	28.04	32.09	35.65	36.40	29.81	32.40	29.18	27.97	28.07	30.16
δEu	1.13	0.96	1.05		1.00	0.96	0.84	0.80	0.85	0.80	0.76	0.84	0.73	0.76	0.76	0.72
δCe	0.85	1.17	0.98		0.85	0.86	0.94	0.79	0.87	0.86	0.93	0.92	0.92	0.87	0.91	0.91

QLM-1, QLM-3, QLM-5, QLM-6, and QLM-9 are granite porphyry. QLM-4 is quartz diorite porphyry. AJS-1, AJS-3, AJS-4, AJS-5, AJS-6, and AJS-9 are granodiorite porphyry. XG-1, XG-2, XG-3, and XG-4 are granodiorite. XG-5, XG-8, and XG-10 are quartz diorite porphyrite. SM-3, SM-4, SM-6, SM-7, SM-10, and SM-13 are granodiorite porphyry. JB-1, JB-2, JB-5, and JB-6 are monzonitic granite. JB-8 and JB-11 are quartz diorite porphyry

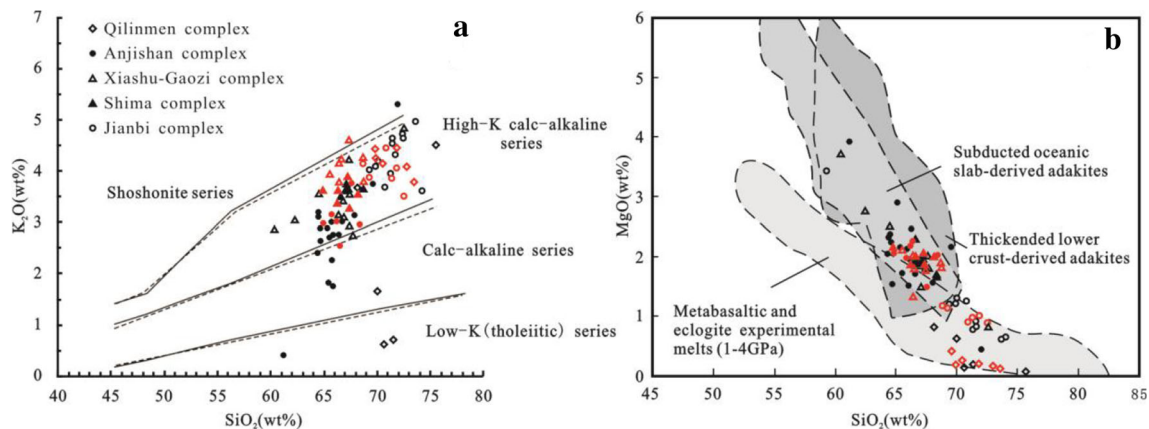


Fig. 5 Selected major element diagrams of **a** K_2O versus SiO_2 (Peccerillo and Taylor 1976; Middlemost 1985) and **b** MgO versus SiO_2 (Defant and Drummond 1990; Atherton and Petford 1993; Ding et al. 2016). Data sources: Qilinmen complexes (Chen 1984; Xia 2000); Anjishan complexes (Chen et al. 1980, 1984; Ning and Chen 1989; Xia 2000; Xu et al. 2001; Zeng et al. 2013); Xiashu–Gaozi complexes (Chen 1984; Xia 2000; Sun 2012); Shima complexes (Chen 1984; Xia 2000; Sun 2012); Jianbi complexes (Yang et al. 1985; Zhu 1987; Zhen and Chen 1988; Xia 2000); and others (Table 2). The reference data are identified by black symbols; our data are marked by red symbols

7 Discussion

7.1 Timing of diagenesis and metallogenesis

The Ningzhen region is an important part of the middle-lower Yangtze River Fe–Cu–Au polymetallic metallogenic belt. Many previous studies have investigated the geology, geochronology, geochemistry, and isotope geochemistry of these magmatic rocks (Xia 2000; Zeng et al. 2013; Wang et al. 2014a, b). The geological and geochronological data show that the Ningzhen Mountains are an important part of the calc-alkaline series in the middle-lower Yangtze River belt, which formed 122–96 Ma. From west to east, this region is composed mainly of six homologous complexes that gradually change in composition from intermediate–acidic to acidic: the Qilinmen, Anjishan, Xiashu–Gaozi, Xinqiao, Shima, and Jianbi complexes (Mao and Zhao 1990). Geochemical research on the trace elements and REE of the five complexes in this study show that the magma source is crust–mantle type in the Ningzhen region, which has the same evolutionary trend.

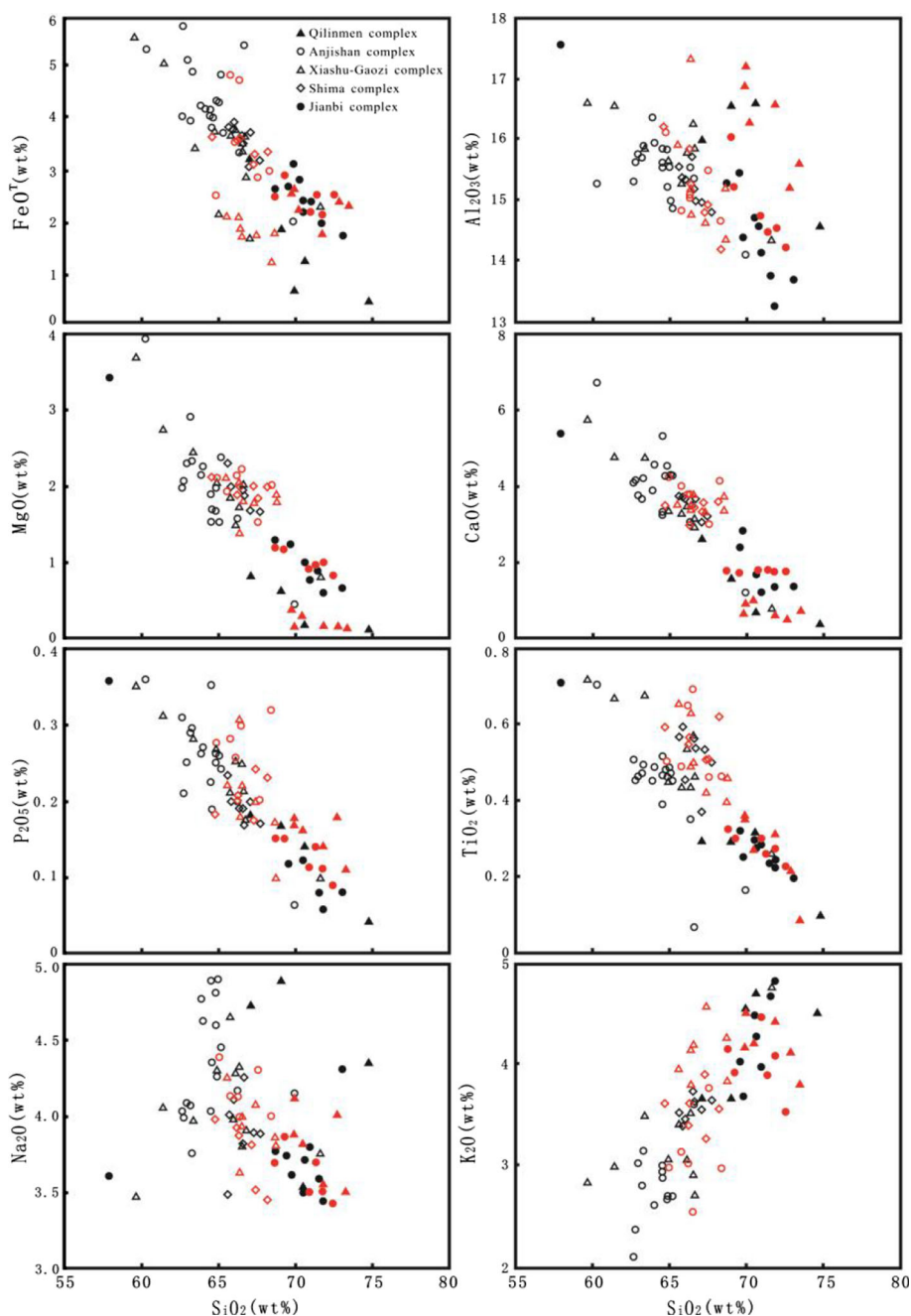
The age of magmatic intrusion in the Ningzhen region reported in literature is variable (Table 3). Regardless of these age differences, the existing geochronological data indicate that the complexes in this region formed during the Early Cretaceous, belonging to the Late Yanshanian. In the present study, LA–ICP–MS zircon U–Pb dating yielded ages of 122.0 ± 1.0 Ma, 106.1 ± 0.8 Ma, 108.7 ± 1.4 Ma, 103.5 ± 1.9 Ma, and 96.8 ± 1.7 Ma for the Qilinmen, Anjishan, Xiashu–Gaozi, Shima, and Jianbi complexes, respectively. The published emplacement ages of the five complexes are ~ 102 , ~ 106 – 109 , ~ 109 , ~ 102 – 103 , and ~ 109 Ma, respectively (Table 3). The formation age of the intermediate–acidic intrusive

complexes is bounded by the above ages. Therefore, it is believed that magmatic emplacement occurred during the Early Cretaceous.

The emplacement sequence of the magmatic rocks is consistent across the Ningzhen region. The results show that the emplacement sequence, from early to late, is diorite porphyrite, quartz diorite porphyrite, granodiorite porphyry, monzonitic granite, and granite (Ning and Chen 1989). The granitoid complex zonation shows a single complex comprised from the edge to the interior phase of quartz diorite porphyrite, quartz monzonite porphyry (granodiorite porphyry), and monzonitic granite (Mao and Zhao 1990). The geological, geochemical, and isotopic characteristics of the intrusive complexes in the Ningzhen region indicate that the diagenetic sequence is augite diorite, diorite or quartz diorite, granodiorite or monzonitic granite, and granite (Chen et al. 1987). The above observations are consistent with the evolution sequence of Bowen’s reaction series. According to the emplacement ages of the five complexes, they decrease in age from west to east and gradually change in composition from neutral to acidic.

Several mineralization ages have been obtained recently in the Ningzhen region. For example, the Anjishan and Tongshan Cu(Mo) deposits show a direct relationship with the Anjishan and Xiashu–Gaozi complexes, respectively (Wang et al. 1997), and the Cishantou skarn iron deposit is related directly to Xiashu–Gaozi complex (Sun et al. 2013). Similarly, the metallogenic age of the Weigang magnetite deposit was reported to be about 102.5 Ma, which is related directly to the Shima complex (Guan et al. 2015). Moreover, the Sm–Nd isochron age of the fluorite of the hydrothermal II stage is 93.7 ± 3.1 Ma, which represents the main ore-forming epoch/stage of the Lunshan gold

Fig. 6 Harker diagrams for samples of the five complexes. The data sources and symbol explanation are the same as those given in Fig. 5



deposit located in the middle of the Anjishan and Shima complexes (Lu et al. 2017). In addition, the Jianbi porphyry Mo(W) deposit is related directly to the Jianbi monzonitic granite (Ma and Wang 2003). Thus far, however, no deposit has shown a direct relationship with related the Qilinmen complex.

The zircon U–Pb dates indicate that Mesozoic intermediate–acidic intrusive complexes in the Ningzhen region were emplaced during the Early Cretaceous, ranging from 109 Ma to 97 Ma. These ages suggest that crystallization of the intermediate–acidic intrusive complexes and

initiation of the mineralization are temporally and possibly genetically related. Therefore, the aforementioned metal deposits belong to one set of the Early Cretaceous polymetallic metallogenic events in the middle-lower Yangtze River metallogenic belt. Thus, we suggest that the Mesozoic large-scale diagenesis and metallogenesis in the Ningzhen region may have ceased 100 Ma or about 95 Ma.

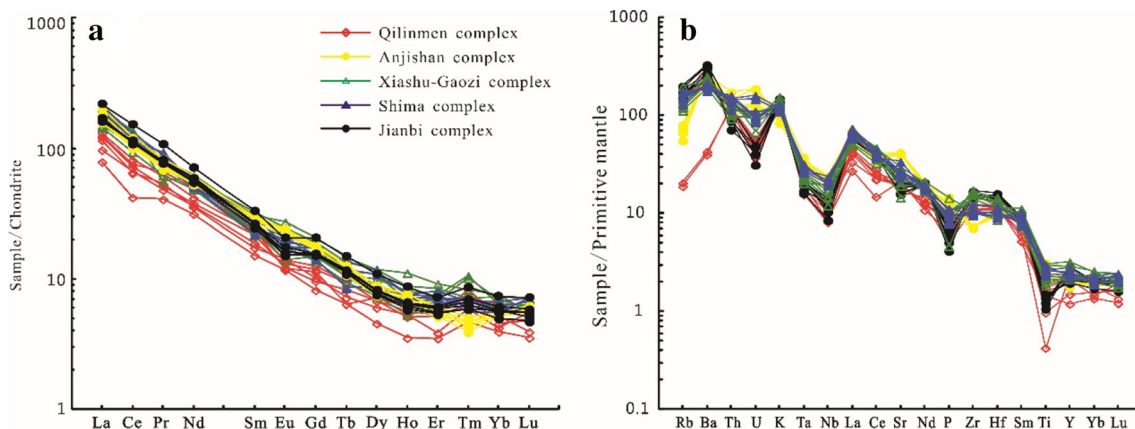


Fig. 7 Chondrite-normalized REE patterns (a) and primitive-mantle-normalized trace element patterns (b). The normalized values are based on Boynton (1984) and Sun and McDonough (1989). Data sources: Qilinmen complexes (Chen et al. 1991); Anjishan complexes (Chen et al. 1991; Xia 2000; Xu et al. 2001; Zhang et al. 2010; Zeng et al. 2013); Xiashu–Gaozi complexes (Chen et al. 1991; Xia 2000; Sun 2012); Shima complexes (Chen et al. 1991; Xia 2000; Sun 2012); Jianbi complexes (Zhen and Chen 1988; Chen et al. 1991; Xia 2000); others (Table 2)

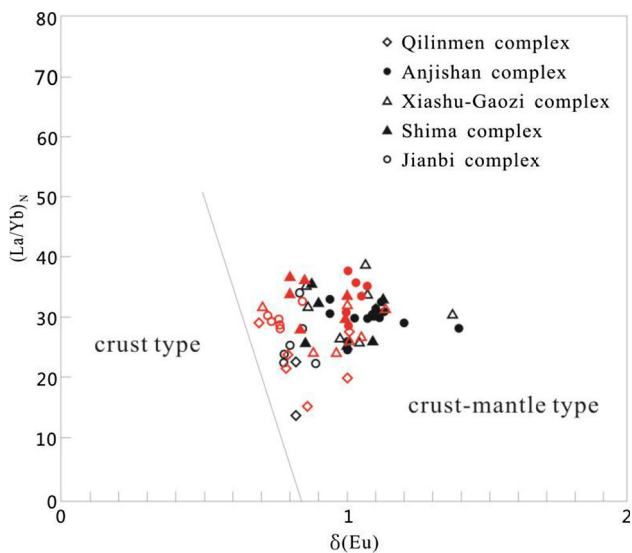


Fig. 8 $(La/Yb)_N$ - $\delta(Eu)$ diagram for the Ningzhen complexes. The data sources are the same as those given in Fig. 7. The reference data are represented by black symbols; our data are shown by red symbols

7.2 Petrogenesis

The Harker diagrams for the five complexes in the Ningzhen region (Fig. 6) indicate that SiO_2 is positively correlated with K_2O . Conversely, SiO_2 is negatively correlated with Na_2O , TiO_2 , Al_2O_3 , FeO^T , MgO , CaO , and P_2O_5 , which reflects that the five complexes have a close genetic relationship and cognate magma evolution. During the magmatic evolution, fractional crystallization of mafic minerals such as pyroxene and hornblende played a major role. The trace element and REE geochemical characteristics also show similarity across the five complexes (Fig. 7), which indicates a common magma source and magmatic evolution.

The REE patterns of the intermediate–acidic complexes are characterized by enrichment in LREE and depletion in HREE in addition to slightly negative or none Eu anomalies (Fig. 7a); the REE patterns exhibit right-inclined curves. The REE patterns also show high $(La/Yb)_N$ ratios, which are in accord with the geochemical signature of adakitic rocks. In summary, the intermediate–acidic complexes in the Ningzhen region are part of the Early Cretaceous adakite succession in eastern China. The intermediate–acidic complexes show chondrite-normalized REE patterns similar to those in samples from Wushan, Lishui, and Ningwu in the middle-lower Yangtze River belt (Gao et al. 2007; Jiang et al. 2008).

In the $(La/Yb)_N$ - $\delta(Eu)$ diagram (Fig. 8), the studied samples all plot in the crust–mantle-type field. This preliminary study indicates that the initial magma formed through interaction of the upper mantle and the crust and then underwent fractional crystallization in the lower crust before being emplaced as intrusive complexes. Therefore, the samples belong to multi-stage homologous intrusive complexes, showing a clear trend in composition from neutral to acidic during their evolution. Ning and Chen (1989) found picotite, anatase, and homologous basic xenoliths in complexes in the Ningzhen region; the $^{87}Sr/^{86}Sr$ ratio in apatite was 0.7066 ± 0.0020 . This evidence also excludes the possibility of the initial magma being directly sourced from the upper mantle or from remelting of crustal sediments.

Geologists divided adakitic rocks into four origin types as follows: (1) adakitic rock produced by direct partial melting of the lower crust (Atherton and Petford 1993); (2) adakitic rock generated by partial melting of delaminated lower crust (Xu et al. 2002; Wang et al. 2004); (3) adakitic rock by differentiation of a basaltic magma at high pressure condition (Castillo et al. 1999; Xiong 2006); (4) adakitic

Table 3 Ages of the complexes in the Ningzhen region

Complex	Lithology	Test method	Age (Ma)	Data sources
Qilinmen	Granite porphyry	U–Pb	102.4 ± 1.2	Chen et al. (2017)
Qilinmen	Granite porphyry	U–Pb	122.0 ± 1.0	This study
Anjishan	Granodiorite porphyry	U–Pb	106.9 ± 0.9	Zeng et al. (2013)
Anjishan	Granodiorite porphyry	U–Pb	108.8 ± 1.2	Liu et al. (2014)
Anjishan	Dioritic porphyry	U–Pb	108.8 ± 1.5	Wang et al. (2014a, b)
Anjishan	Granodiorite porphyry and quartz diorite	U–Pb	107.0 – 108.0	Guan et al. (2015)
Anjishan	Granodiorite porphyry	U–Pb	106.1 ± 0.8	This study
Xiashu-Gaozi	Quartz diorite porphyrite	U–Pb	109.1 ± 1.9	Sun et al. (2013)
Xiashu-Gaozi	Quartz diorite porphyrite	U–Pb	108.7 ± 1.4	This study
Shima	Granodiorite	U–Pb	101.6 ± 1.1	Sun et al. (2013)
Shima	Quartz diorite porphyrite	U–Pb	102.5 ± 1.1	Guan et al. (2015)
Shima	Granodiorite porphyry	U–Pb	103.5 ± 1.9	This study
Jianbi	Monzonitic granite	U–Pb	109.3 ± 1.1	Chen et al. (2017)
Jianbi	Monzonitic granite	U–Pb	96.8 ± 1.7	This study

rock by magma mixing (Guo et al. 2007; Chen et al. 2013). In this study, the major element geochemical characteristics of the complexes were high SiO₂ content and relatively high MgO and Al₂O₃ contents. These complexes also display significant positive Sr anomalies and negative Ta, Nb, and Ti anomalies. In addition, the geochemical characteristics of the trace elements in the five complexes were as follows: the chondrite-normalized REE patterns were basically similar, exhibiting right-inclined curves. The patterns had high (La/Yb)_N ratios and slightly negative Eu anomalies. The primitive-mantle-normalized trace element patterns were also similar in that they were rich in LILE including Rb, Ba, and K and low in HFSE such as Nb, Ta, P, and Ti. The geochemical characteristics of these major and trace elements indicate that the process of magmatic evolution is consistent in the Ningzhen region. The complexes from this region have high Mg# (> 50) (Wang et al. 2014a, b; Xu et al. 2014), high Sr/Y ratios coupled with low Y (Xu et al. 2002; Wang et al. 2014a, b), low $\epsilon_{\text{Nd}(t)}$ values (26.8–29.7) and ¹⁴³Nd/¹⁴⁴Nd ratios < 0.5123 (Xu et al. 2002), and high ⁸⁷Sr/⁸⁶Sr ratios (0.7053–0.7066) (Ning and Chen 1989; Xu et al. 2002). These characteristics are inconsistent with origins from slab melting or plate subduction. Previous studies have suggested that the lithosphere in eastern China was thick in the Mesozoic, measuring more than ~ 40 km in Ningzhen region before the underplating of basaltic magma and delamination of the lower crust occurred (Xu and Ma 2003; Wu et al. 2007). At the latter stage, the crust began to thin gradually before reaching the present thickness of approximately 30 km as measured by geophysical techniques (Wang and Li 1992). Thus, we infer that the lower crust subsided into the underlying mantle, and the lower crust which entered the

mantle partially melted to form adakitic melt. As this adakitic melt then ascended, the MgO content and Mg# value of the adakitic rocks increased from interaction with mantle rocks. This led us to conclude that the adakitic rocks most likely originated from the partial melting of the delaminated lower crust.

7.3 Geodynamic setting

The difference in crustal thickness indicates that the lithosphere of eastern China has been thinned since the Mesozoic. A thick overriding plate is favorable for the formation of magmatic rocks over volcanic rocks. Moreover, it favors magma evolution and prevents the leakage of magmatic fluids, both of which promote porphyry deposits (Sun et al. 2017a, b, c). A summary by Mao et al. (2003) suggests that large-scale mineralization in the North China Craton and its adjacent areas occurred during three periods: 200–160, 140, and 130–110 Ma. It is proposed that the geodynamic setting of the third period is related to the thinning of the lithosphere, which is directly related to our discussion. Although the occurrence time and mechanism of the lithospheric thinning events are still under debate, most geologists believe that the interaction between the Paleo-Pacific Plate and the overlying continental crust was the main driving force of lithospheric thinning in eastern China (Mao et al. 2003; Wu et al. 2003; Sun et al. 2007). The lithospheric thinning events should have a starting time, a maximum thinning time, and an end time; thus, the time constraint is indirect (Wu et al. 2003). The peak periods of lithospheric thinning may correspond to the most intense periods of diagenesis and mineralization. Although dating of the lithospheric thinning events remains

controversial, the zircon U–Pb dating of the five magmatic rocks are in the third large-scale mineralization (130–110 Ma), and the lithosphere of Ningzhen region thinned during the formation of five magmatic rocks.

We suggest that the Late Mesozoic in eastern China, which includes the Ningzhen region, was a period of tectonic regime transformation. The area was influenced by a change in the tectonic regime of the Pacific Plate, resulting in a transformation from a compressional to extensional setting and the associated reduction in crustal thickness (Wu et al. 2003). After thinning, the gravitational instability of the lithosphere increased and led to deep lithospheric mantle and lower crust delamination followed by large-scale asthenospheric upwelling. The basic magma then intruded into the base of the lower crust, leading to partial melting and magma mixing in the lower crust. Eventually, the magma was emplaced and formed a crust-mantle type complex. During the process of lower crust delamination, if granitic magma was generated and emplaced into the upper crust, the resulting granitic rocks could have trace element signatures. For example, during the crystallization of partial melting relics under high-pressure conditions, the ratios of La/Yb in magma should be high owing to the remnants of garnet and hornblende (Xu and Qiu 2010); this corresponds to the high ratios of $(La/Yb)_N$ found in the five complexes in this study.

Previous geochronological studies conducted on the Yanshanian magmatic rocks in the middle-lower Yangtze River belt concluded that three main periods of mineralization occurred (Wu et al. 2005; Xie et al. 2008). The first period of magmatic activity occurred 145–136 Ma (Zhou et al. 2007; Wu et al. 2012; Wang et al. 2015, 2016; Duan and Jiang 2018) when magmatic rocks were formed mainly in the southeast regions of Hubei, Tongling, and Anqing. The second period occurred between 135 and 127 Ma (Zhou et al. 2008a, b, 2013; Nie et al. 2017; Sun et al. 2017a, b, c; Liu et al. 2018) when magmatic rocks were produced mainly in the Luzong and Ningwu basins. The third period occurred between 126 and 123 Ma (Lou and Du 2006; Fan et al. 2008; Yuan et al. 2010; Su et al. 2013) when magmatic rocks were produced in areas of fault-related uplift and in fault-controlled basins, mainly in the Fanchang and Ningwu basins. These three periods of magmatism show that the Mesozoic magmatic rock emplacement ages in the middle-lower Yangtze River belt decrease in age from south to north. The Ningzhen region is located in the easternmost part of the middle-lower Yangtze River Cu–Fe polymetallic metallogenic belt. Thus, magmatic emplacement may have occurred after the three periods described above. Zeng et al. (2013) dated samples from the Anjishan complex by using sensitive high-resolution ion microprobe (SHRIMP) zircon U–Pb dating. They found that the lithospheric thinning events in

the Ningzhen region may have occurred ~ 20 Ma later than that in the southeast Hubei and Tongling regions and that lithospheric delamination in the Ningzhen region may have continued until ~ 107 Ma. Wang et al. (2014a, b) dated the Anjishan, Xiashu–Gaozi, and Shima complexes by using LA–ICP–MS zircon U–Pb methods. Considering the tectonic evolution of the Pacific Plate and the age constraints on diagenesis and mineralization in eastern China since the Cretaceous, Wang et al. (2014a, b) proposed that the lithospheric thinning in the middle-lower Yangtze River belt began ~ 135 Ma and may have continued until ~ 100 Ma. Through comprehensive consideration of the previous research results given above and the results of the present study, we agree that the diagenesis and mineralization in the Ningzhen region belong to the final period of mineralization in the Mesozoic. Therefore, a new period of large-scale diagenetic and metallogenic events has been identified, which is of great significance to the study of the tectonic, magmatic, and mineralization history of the middle-lower Yangtze River metallogenic belt.

In this paper, the Jianbi complex was dated to 96.8 ± 1.7 Ma using LA–ICP–MS zircon U–Pb methods. The ages of the Qilinmen complex, at ~ 99 –122 Ma, the Anjishan complex, at ~ 106 –112 Ma, the Xiashu–Gaozi complex, at ~ 106 –109 Ma, and the Shima complex, at ~ 82 –109 Ma, have been reported. On the basis of these ages, we conclude that the magmatic emplacement coincided with the period of Cu–Fe mineralization. As previously described, the third period of magmatic activity in the Ningzhen region ended at 123 Ma, with an interval of 17–23 Ma between the start of the period and the peak magmatism at 100–106 Ma. Therefore, we propose that important large-scale diagenesis and mineralization occurred after the three large-scale diagenetic and metallogenic periods, with emplacement times between 110 and 95 Ma. Large-scale diagenesis and mineralization in the Mesozoic Ningzhen region of eastern China may have continued until 100 Ma or 95 Ma; however, further study is required to confirm this finding.

8 Conclusions

The results of this study are summarized below:

- (1) We determined the zircon U–Pb ages with LA–ICP–MS for the Qilinmen, Anjishan, Xiashu–Gaozi, Shima, and Jianbi complexes to be 122.0 ± 1.0 Ma, 106.1 ± 0.8 Ma, 108.7 ± 1.4 Ma, 103.5 ± 1.9 Ma, and 96.8 ± 1.7 Ma, respectively. It is suggested that the intermediate–acidic intrusive complexes in the Ningzhen region were emplaced

during the Early Cretaceous. The major element characteristics of the five complexes show that the lithology changes from neutral to acidic from west to east.

- (2) The SiO_2 values in the Ningzhen complexes positively correlate with K_2O . Conversely, SiO_2 negatively correlates with Na_2O , TiO_2 , Al_2O_3 , FeO^T , MgO , CaO , and P_2O_5 , which indicates a close genetic relationship among the five complexes. The chondrite-normalized REE and primitive-mantle-normalized trace element patterns also show similarities. The trace element geochemical results show enrichment of LILE and depletion of HFSE, and samples from all five complexes are classified as crust-mantle type igneous rock. Therefore, we conclude that the adakitic rocks in the Ningzhen region are of crust-mantle type and can be classified as multi-stage homologous intrusive complexes.
- (3) The ages of the intermediate–acidic intrusive complexes are as follows: Qilinmen, ~ 99 – 117 Ma; Anjishan, ~ 106 – 112 Ma, Xiashu–Gaozi, ~ 106 – 109 Ma, Shima, ~ 82 – 109 Ma, and Jianbi, ~ 100 – 102 Ma. These ages coincide with the Cu–Fe mineralization period. Therefore, we conclude that large-scale Mesozoic diagenesis and mineralization in the Ningzhen region in eastern China may have continued until 100 Ma or ~ 95 Ma.

Acknowledgements The study was financially supported by the Major State Basic Research Development Program of China (973 Program) (No. 2014CB440906).

References

- Atherton MP, Petford N (1993) Generation of sodium-rich magmas from newly underplated basaltic crust. *Nature* 362:144–146
- Black LP, Kamo SL, Williams IS, Mundil R, Davis DW, Korsch RJ, Foudoulis C (2003) The application of SHRIMP to Phanerozoic geochronology, a critical appraisal of four zircon standards. *Chem Geol* 200:171–188
- Boynton WV (1984) Cosmochemistry of the rare earth elements: meteorite studies. In: Henderson P (ed) *Rare earth element geochemistry*, 1st edn. New York, pp 63–114 <https://doi.org/10.1016/B978-0-444-42148-7.50008-3>
- Bureau of Geology and Mineral Exploration of Jiangsu Province (1989) *Geological records of Ningzhen mountain range*. Phoenix Science Press, Nanjing (in Chinese)
- Castillo PR, Janney PE, Solidum R (1999) Petrology and geochemistry of Camiguin Island, southern Philippines: insights into the source of adakite and other lavas in a complex arc tectonic setting. *Contrib Miner Petrol* 134:33–51
- Castro A, Moreno VI, Rosa JD (1991) H-type (hybrid) granitoids: a proposed revision of the granite-type classification and nomenclature. *Earth-Sci Rev* 31(3–4):237–253
- Chen JD (1984) Basic features of three Yanshanian composite rock masses in Jiangsu province and their ore bearing characters. *Reg Geol of China* 9:17–31 (in Chinese with English abstract)
- Chen SS, Wei JS, Yang NQ, Chen SD (1980) The geochemical characteristics of mineral rocks of Anjishan copper. *Geol Prospect* 5:24–30 (in Chinese)
- Chen SY, Mao JR, Su YX, Zhao SL, Cheng QF (1987) Geochemical characteristics of Mesozoic intrusive rock in south Jiangsu province. *Bull Nanjing Inst Geol Miner Resour, Chin Acad Geol Sci* 8:46–57 (in Chinese with English abstract)
- Chen SS, Tao WS, Chen GS (1991) Geochemistry of rare earth elements of intrusive rocks in Nanjing–Zhenjiang Mountains. *Geol Jiangsu* 4:193–199 (in Chinese with English abstract)
- Chen B, He JB, Ma XH (2009) Petrogenesis of mafic enclaves from the north Taihang Yanshanian intermediate to felsic plutons: evidence from petrological, geochemical and zircon Hf–O isotopic data. *Sci China Ser D-Earth Sci* 39(7):922–934 (in Chinese with English abstract)
- Chen B, Jahn BM, Suzuki K (2013) Petrological and Nd–Sr–Os isotopic constraints on the origin of high-Mg adakitic rocks from the North China Craton: tectonic implications. *Geology* 41:91–94
- Chen ZH, Zhao L, Li YN (2017) Zircon U–Pb ages of ore-free intrusions in the Ningzhen metallogenic district of the Middle-Cambrian Yangtze River metallogenic belt and their geological significances. *Bull Miner, Petrol Geochem* 36(1):171–178 (in Chinese with English abstract)
- Defant MJ, Drummond MS (1990) Derivation of some modern arc magmas by melting of young subducted lithosphere. *Nature* 347:662–665
- Ding HX, Hou QY, Zhang ZM (2016) Petrogenesis and tectonic significance of the Eocene adakite-like rocks in western Yunnan, southeastern Tibetan Plateau. *Lithos* 245:161–173
- Duan DF, Jiang SY (2018) Using apatite to discriminate synchronous ore-associated and barren granitic rocks: a case study from the Edong metallogenic district, South China. *Lithos*. Accepted 1 May 2018 (in press)
- Dubé B, Dunning GR, Lauzière K, Roddick JC (1996) New insights into the appalachian orogen from geology and geochronology along the Cape Ray fault zone, southwest Newfoundland. *Geol Soc Am Bull* 108:101–116
- Fan Y, Zhou TF, Yuan F, Qian CC, Lu SM, David C (2008) LA-ICP-MS zircon U–Pb ages of the A-type granites in the Lu–Zong (Lujiang–Zongyang) area and their geological significances. *Acta Petrol Sin* 24:1715–1724 (in Chinese with English abstract)
- Gao XF, Guo F, Li CW, Cai GQ (2007) The genesis of two types of Late Mesozoic intermediate-felsic volcanic rocks in Lishui Basin, Lower Yangtze valley. *Acta Petrol Miner* 26:1–12 (in Chinese with English abstract)
- Guan JP, Wei FB, Sun GX, Huang JP, Wang LJ (2015) Zircon U–Pb dating of intermediate-acid intrusive rocks in the middle section of Ningzhen district and their metallogenic implications. *Geotecton Metal* 39(2):344–354 (in Chinese with English abstract)
- Guo F, Nakamura E, Fan WM, Kobayoshi K, Li CW (2007) Generation of Paleocene adakitic and esites by magma mixing, Yanji Area, NE China. *J Petrol* 48:661–692
- Hoskin PWO, Black LP (2000) Metamorphic zircon formation by solid-state recrystallization of protolith igneous zircon. *J Metamorph Geol* 18:423–439
- Jiang SY, Li L, Zhu B, Ding X, Jiang YH, Gu LX, Ni P (2008) Geochemical and Sr–Nd–Hf isotopic compositions of granodiorite from the Wushan copper deposit, Jiangxi Province and their implications for petrogenesis. *Acta Petrol Sin* 24:1679–1690 (in Chinese with English abstract)
- Liu BJ, Li TD (2001) Some problems of geology. *Adv Earth Sci* 16(5):607–616 (in Chinese with English abstract)
- Liu YS, Hu ZC, Gao C, Gao S, Günther D, Xu JF, Chen H (2008) In situ analysis of major and trace elements of anhydrous

- minerals by LA-ICP-MS without applying an internal standard. *Chem Geol* 257:34–43
- Liu YS, Gao S, Hu ZC, Gao C, Zong K, Wang D (2010a) Continental and oceanic crust recycling-induced melt–peridotite interactions in the Trans-North China Orogen: U–Pb dating, Hf isotopes and trace elements in zircons from mantle xenoliths. *J Petrol* 51:537–571
- Liu YS, Hu ZC, Zong KQ (2010b) Reappraisal and refinement of zircon U–Pb isotope and trace element analyses by LA-ICP-MS. *Chin Sci Bull* 55(15):1535–1546
- Liu JM, Yan J, Li QZ, Liu XQ (2014) Zircon LA-ICPMS dating of the Anjishan pluton in Nanjing–Zhenjiang area and its significance. *Geol Rev* 60(1):190–199 **(in Chinese with English abstract)**
- Liu YN, Fan Y, Zhou TF, Zhang LJ, White NC, Hong HL, Zhang W (2018) LA-ICP-MS titanite U–Pb dating and mineral chemistry of the Luohe magnetite-apatite (MA)-type deposit in the Lu–Zong volcanic basin, Eastern China. *Ore Geol Rev* 92:284–296
- Lou YE, Du YS (2006) Characteristics and zircon SHRIMP U–Pb ages of the Mesozoic intrusive rocks in Fanchang, Anhui province. *Geochimica* 35:359–366 **(in Chinese with English abstract)**
- Lu BC, Yu JJ, Chen CS, Wang TZ, Che LR, Lu ZY, Yin LQ (2017) Study of fluid inclusions, stable isotopes and geochronology of Lunshan gold deposit, Jiangsu province. *Miner Depos* 36(3):675–690 **(in Chinese with English abstract)**
- Ludwig KR (2003) User's Manual for Isoplot 3.00, a geochronological Toolkit for Microsoft Excel. Berkeley Geochronological Center Special Publication, No. 4, pp 25–32
- Ma C, Wang SJ (2003) Features of Jianbi rock mass and type of molybdenum (wolframium) deposits, in Zhejiang, Jiangsu province. *Jiangsu Geol* 27(3):152–158 **(in Chinese with English abstract)**
- Mao JR, Zhao SL (1990) Chemical evolution of magma in batholith of Nanjing–Zhenjiang Mountain. *Bull Nanjing Inst Geol Miner Resour, Chin Acad Geol Sci* 11:15–28 **(in Chinese with English abstract)**
- Mao JW, Wang YT, Zhang ZH, Yu JJ, Niu BG (2003) Geodynamic settings of Mesozoic large-scale mineralization in North China and adjacent areas -Implication from the highly precise and accurate ages of metal deposits. *Sci China (Ser D)* 46:839–849
- Mao JW, Wang YT, Lehmann B (2006) Molybdenite Re–Os and albite $^{40}\text{Ar}/^{39}\text{Ar}$ dating of Cu–Au–Mo and magnetite porphyry systems in the Yangtze River Valley and metallogenic implications. *Ore Geol Rev* 29(3–4):307–324
- Mao JW, Xie GQ, Duan C, Pirajno F, Ishiyama D, Chen YC (2011) A tectono-genetic model for porphyry–skarn–stratabound Cu–Au–Mo–Fe and magnetite-apatite deposits along the Middle-Lower Yangtze River valley, eastern China. *Ore Geol Rev* 43(1):294–314
- Martin H (1999) Adakitic magmas: modern analogues of Archaean granitoids. *Lithos* 46:411–429
- Middlemost EAK (1985) *Magmas and magmatic rocks*. Longman, London
- Nguyen H, Kozo U (2003) Geochemistry of Cenozoic basalts in the Fukuoka district (northern Kyushu, Japan): implications for asthenosphere and lithospheric mantle interaction. *Chem Geol* 198(3–4):249–268
- Nie LQ, Zhou TF, Fan Y, Zhang LJ, Cooke DR, White NC (2017) Geology, geochemistry and genesis of the Makou magnetite-apatite deposit in the Luzong volcanic basin, Middle-Lower Yangtze River Valley Metallogenic Belt, Eastern China. *Ore Geol Rev* 91:264–277
- Ning RZ, Chen GS (1989) REE characteristics of Yanshanian intrusive rocks from Ningzhen. *Geochimica* 1:52–61 **(in Chinese with English abstract)**
- Pan YM, Dong P (1999) The Lower Changjiang (Yangzi/Yangtze River) metallogenic belt, East China: intrusion and wall rock-hosted Cu–Fe–Au, Mo, Zn, Pb, Ag deposits. *Ore Geol Rev* 15(4):177–242
- Peccerillo R, Taylor R (1976) Geochemistry of Eocene calc-alkaline volcanic rocks from the Kastamonu area, Northern Turkey. *Contrib Miner Petrol* 58:63–81
- Romeo I, Lunar R, Capote R, Quesada C, Dunning GR, Pina R, Ortega L (2006) U–Pb age constraints on Variscan magmatism and Ni–Cu–PGE metallogeny in the Ossa–Morena Zone (SW Iberia). *J Geol Soc* 163:837–846
- Rudnick RL, Gao S (2003) Composition of the continental crust. In: Heinrich DH, Turekain KK (eds) *Treatise on geochemistry*, vol 3. Pergamon, Oxford, pp 1–64
- Su YP, Zheng JP, Griffin WL, Zhao JH, Reilly SY, Tang HY, Ping XQ, Xiong Q (2013) Petrogenesis and geochronology of Cretaceous adakitic, I- and A-type granitoids in the NE Yangtze block: constraints on the eastern subsurface boundary between the North and South China blocks. *Lithos* 175–176:333–350
- Sun Y (2012) Origin of Late Mesozoic intrusive rocks in Ningzhen, Jiangsu Province and Their Relationship with Mineralization. China University of Geosciences, Wuhan **(in Chinese)**
- Sun SS, McDonough WF (1989) Chemical and isotopic systematics of oceanic basalts: implications for mantle composition and processes. *Geol Soc Lond Spec Publ* 42:313–345
- Sun WD, Ding X, Hu YH, Li XH (2007) The golden transformation of the Cretaceous plate subduction in the west Pacific. *Earth Planet Sci Lett* 262:533–542
- Sun Y, Ma CQ, Liu YY (2013) The latest Yanshanian magmatic and metallogenic events in the Middle-Lower Yangtze River belt: evidences from the Ningzhen region. *Chin Sci Bull* 58(34):4308–4318
- Sun J, Zhao JY, Nie AG (2017a) Zircon U–Pb dating and whole-rock elemental geochemistry of the Shazi anatase deposit in Qinglong, Western Guizhou, SW China. *Acta Geochim* 36(2):329–338
- Sun WA, Yuan F, Jowitt SM, Zhou TF, Hollings P, Liu GX, Li XH (2017b) Geochronology and geochemistry of the Fe ore-bearing Zhonggu intrusions of the Ningwu Basin: implications for tectonic setting and contemporaneous Cu–Au mineralization in the Middle-Lower Yangtze Metallogenic Belt. *Ore Geol Rev* 84:246–272
- Sun WD, Wang JT, Zhang LP, Zhang CC, Li H, Ling MX, Ding X, Li CY, Liang HY (2017c) The formation of porphyry copper deposits. *Acta Geochim* 36(1):9–15
- Wang QS, Li JL (1992) Study on the structure and evolution of continental lithosphere in southeastern China. Science and Technology of China Press, Beijing **(in Chinese)**
- Wang LB, Ji KJ, Chen D (1997) Re–Os isotope ages of molybdenite from the Anjishan copper deposit and the Tongshan copper-molybdenum deposit and their implications. *Acta Petrol Miner* 16:59–64 **(in Chinese with English abstract)**
- Wang Q, Zhao ZH, Jian P, Xu JF, Bao ZW, Ma JL (2004) SHRIMP zircon geochronology and Nd–Sr isotopic geochemistry of the Dexing granodiorite porphyries. *Acta Petrol Sin* 20(2):315–324 **(in Chinese with English abstract)**
- Wang FY, Liu SA, Li SG, Akhtar S, He YS (2014a) Zircon U–Pb ages, Hf–O isotopes and trace elements of Mesozoic high Sr/Y porphyries from Ningzhen, eastern China: constraints on their petrogenesis, tectonic implications and Cu mineralization. *Lithos* 200–201:299–316
- Wang XL, Zeng JN, Ma CQ, Li XF, Wu YF, Lu SF (2014b) Zircon U–Pb dating of Yanshanian intrusive rocks in Ningzhen District, Jiangsu: the chronology evidence for a new stage of petrogenesis and metallogeny in the middle and lower reaches of Yangtze

- River. *Earth Sci Front* 21:289–301 **(in Chinese with English abstract)**
- Wang SW, Zhou TF, Yuan F, Fan Y, Zhang LJ, Song YL (2015) Petrogenesis of Dongguashan skarn–porphyry Cu–Au deposit related intrusion in the Tongling district, eastern China: geochronological, mineralogical, geochemical and Hf isotopic evidence. *Ore Geol Rev* 64:53–70
- Wang SW, Zhou TF, Yuan F, Fan Y, Cooke DR, Zhang LJ, Fu B, White NC (2016) Geochemical characteristics of the Shujiadian Cu deposit related intrusion in Tongling: petrogenesis and implications for the formation of porphyry Cu systems in the Middle-Lower Yangtze River Valley metallogenic belt, eastern China. *Lithos* 252–253:185–199
- Wu FY, Ge WC, Sun DY, Guo CL (2003) Discussions on the lithospheric thinning in eastern China. *Earth Sci Front* 10:51–60 **(in Chinese with English abstract)**
- Wu FY, Lin JQ, Wilde SA, Zhang XO, Yang JH (2005) Nature and significance of the Early Cretaceous giant igneous event in eastern China. *Earth Planet Sci Lett* 233(1–2):103–119
- Wu FY, Li XH, Yang JH, Zheng YF (2007) Discussions on the petrogenesis of granites. *Acta Petrol Sin* 23:1217–1238 **(in Chinese with English abstract)**
- Wu FY, Ji WL, Sun DH, Yang YH, Li XH (2012) Zircon U–Pb geochronology and Hf isotopic compositions of the Mesozoic granites in southern Anhui Province, China. *Lithos* 150(1):6–25
- Xia JS (2000) A preliminary division of lineage units of granitoid rocks in Ning-Zhen region. *Geology of Jiangsu* 24:81–86 **(in Chinese with English abstract)**
- Xie GQ, Mao JW, Li RL, Bierlein FP (2008) Geochemistry and Nd–Sr isotopic studies of Late Mesozoic granitoids in the southeastern Hubei Province, Middle-Lower Yangtze River belt, eastern China: petrogenesis and tectonic setting. *Lithos* 104(1–4):216–230
- Xiong XL (2006) Trace element evidence of the growth of early continental crust by melting of rutile-bearing hydrous eclogite. *Geology* 34:945–948
- Xu JH, Ma CQ (2003) Constraints of experimental petrology on the origin of adakites, and petrogenesis of Mesozoic K–rich and high Sr/Y ratio granitoids in eastern China. *Earth Sci Front* 10:417–427 **(in Chinese with English abstract)**
- Xu XS, Qiu JS (2010) *Igneous petrology*. Science Press, Beijing **(in Chinese)**
- Xu JF, Wang Q, Xu YG, Zhao ZH, Xiong XL (2001) Geochemistry of Anjishan intermediate-acid intrusive rocks in Ningzhen area: constraint to origin of the magma with HREE and Y depletion. *Acta Petrol Sin* 17:576–584 **(in Chinese with English abstract)**
- Xu JF, Shinjo R, Defant MJ, Wang Q, Rapp RP (2002) Origin of Mesozoic adakitic intrusive rocks in the Ningzhen area of east China: partial melting of delaminated lower continental crust? *Geology* 30(12):1111–1114
- Xu JF, Wu JB, Wang Q, Chen JL, Cao K (2014) Research advances of adakites and adakitic rocks in China. *Bull Miner Petrol Geochem* 33(1):6–13 **(in Chinese with English abstract)**
- Yang SS, Duan JC, Ju ZF, He JG (1985) Discussion on geological characteristics and genetic mechanism of Jianbi W–Mo deposit. *Geol Prospect* 8:20–27 **(in Chinese)**
- Yuan F, Zhou TF, Fan Y, Huang YM, Zhang LJ (2010) LA–ICP MS U–Pb ages of zircons from Mesozoic volcanic rocks and their significance in Fanchang basin, Anhui Province, China. *Acta Petrol Sin* 26(9):2805–2817 **(in Chinese with English abstract)**
- Zeng JN, Li JW, Chen JH, Lu JP (2013) SHRIMP zircon U–Pb dating of Anjishan intrusive rocks in Ningzhen district, Jiangsu, and its geological significance. *Earth Science—Journal of China University of Geosciences* 38:57–67 **(in Chinese with English abstract)**
- Zhang SG, Li GX, Shi DF, Han SL (2010) REE geochemistry research of Yanshanian ore-forming system in Ningzhen skarn deposit area. *J Chin Rare Earth Soc* 28:626–632 **(in Chinese with English abstract)**
- Zhen YQ, Chen JX (1988) An approach to the genesis of the granite type molybdenum deposits in Jianbi, Jiangsu. *J Guilin Coll Geol* 8:353–366 **(in Chinese with English abstract)**
- Zhou TF, Yuan F, Yue SC, Liu XD, Zhang X, Fan Y (2007) Geochemistry and evolution of ore-forming fluids of the Yueshan Cu–Au skarn- and vein-type deposits, Anhui Province, South China. *Ore Geol Rev* 31(2):279–303
- Zhou TF, Fan Y, Yuan F (2008a) Advances on petrogenesis and metallogeny study of the mineralization belt of the Middle and Lower Reaches of the Yangtze River area. *Acta Petrol Sin* 24:1665–1678 **(in Chinese with English abstract)**
- Zhou TF, Fan Y, Yuan F, Lu SM, Shang SG, Cooke D, Meffre S, Zhao GC (2008b) Geochronology of the volcanic rocks in the Lu–Zong basin and its significance. *Sci China (Ser D)* 51(10):1470–1482
- Zhou TF, Fan Y, Yuan F, Zhang LJ, Qian B, Ma L, Yang XF (2013) Geology and geochronology of magnetite-apatite deposits in the Ning–Wu volcanic basin, eastern China. *J Asian Earth Sci* 66:90–107
- Zhu ZQ (1987) Analysis of the metallogenic characteristics of skarn scheelite deposit in the middle and lower Yangtze River. *Geol Jiangsu* 3:8–11 **(in Chinese)**